ANL/FPP/TM--162

DE83 009478

Distribution Categories:
Magnetic Fusion Energy (UC-20)
MFE—Fusion Systems (UC-20d)

ANL/FPP/TM-162

ARGONNE NATIONAL LABORATORY
9700 South Cass Avenue
Argonne, Illinois 60439

ALTERNATE-FUEL REACTOR STUDIES

by

K. Evans, Jr., D. A. Ehst, Y. Gohar, J. Jung,
R. F. Mattas, and L. R. Turner

Fusion Power Program

J. G. Gilligan

Fusion Studies Laboratory
University of Illinois
Urbana, Illinois 68801

February 1983

DISCLAIMER

TABLE OF CONTENTS

LIST OF FIGURES

LIST OF TABLES

ACKNOWLEDGMENTS

Cyrilla Hytry was responsible for the typing and final assembly of this report.

ALTERNATE-FUEL REACTOR STUDIES

K. Evans, Jr., D. A. Ehst, J. G. Gilligan, Y. Gohar,
J. Jung, R. F. Mattas, and L. R. Turner

Fusion Power Program
Argonne National Laboratory
Argonne, Illinois 60439

ABSTRACT

A number of studies related to improvements and/or greater understanding of alternate-fueled reactors is presented. These studies cover the areas of non-Maxwellian distributions, materials and lifetime analysis, a ^{3}He-breeding blanket, tritium-rich start-up effects, high field magnet support, and reactor operation spanning the range from full D-T operation to operation with no tritium breeding.

Chapter 1

INTRODUCTION

1. INTRODUCTION

This report covers several, somewhat independent studies related to alternate-fueled reactors. These studies were carried on during FY 1982 in the Fusion Power Program at Argonne National Laboratory. The issues covered arose from the WILDCAT study as areas where improvements could be made or where more study was required in order to develop a better understanding of the particular design issue.

1.1 Non-Maxwellian Distributions

The first topic deals with the possibility of enhancing the low fusion power density typical of alternate-fueled reactors, probably their most important shortcoming, by providing a non-Maxwellian distribution of fuel ions. The case considered is that in which the non-Maxwellian distribution is provided by fundamental ion-cyclotron resonance heating (ICRH), where the theory is known to have good experimental verification.

This ICRH heating raises the tail of the distribution and also the average energy. To compare the power density of a tokamak reactor operating at its beta limit, it is then necessary to take into account that the density must be decreased to make up for the increased energy, partially offsetting the benefit of the non-Maxwellian distribution. In this study this effect has been taken into account, and the resulting values of $\langle\sigma v\rangle/T^2$, where T is the effective temperature, have been calculated and compared. The fact that the beta limit may be different for the non-Maxwellian distribution has been noted but not treated.

It is found that there is an optimum amount of ICRH heating. If the heating is too large, the increase in effective temperature completely offsets the benefits of the redistribution of ions. Enhancements of up to 40% have been calculated, depending on the effective temperature of the distribution. The largest enhancements occur at lower values of the effective temperature. For high values there is no increase in $\langle\sigma v\rangle/T^2$ over a Maxwellian distribution. It is not clear that the enhancement obtained creates more fusion power than is needed to provide the ICRH heating, and study of higher harmonic ICRH heating, which may be more beneficial, is recommended.

As a side benefit of this study, errors in two widely distributed formulae for approximation by the fusion corss sections have been found and corrected.

1.2 ^{3}He Breeding Blanket

The possibiity of breeding ^{3}He rather than tritium in a fusion reactor blanket has been considered as a new and innovative idea. However, it was found that for the material with the largest (n,^{3}He) cross section (i.e. calcium), the ^{3}He production rate was still too small to be of practical interest.

1.3 Materials Analysis

A one-dimensional materials lifetime code has been upgraded and a more extensive analysis of the WILDCAT first wall has been performed. The lifetime code calculates the temperature, stress, and strain distributions through a plate with specified constraints based on the reactor operating and design parameters, then calculates the property changes of the materials and the effects of those changes on the distributions, repeating until failure occurs or the desired lifetime is reached.

The code has been expanded to allow a dual material plate, representative of a wall with a low-Z coating bonded to a structural material. In addition, a totally constrained plate has been considered for the WILDCAT first wall in addition to a plate that can expand but not bend as treated in Ref. 1. The two conditions should span the possible range of constraints for the wall.

The results of the more sophisticated and extended analysis are that for normal operation the WILDCAT first wall design should achieve a 20-y lifetime regardless of the plate constraint. The primary limit on the liftime is the sputtering loss of the beryllium cladding. For the lesser constrained plate the stresses are low, and the lifetime could probably be substantially increased by increasing the beryllium thickness. It is probably not advisable, however, to extend the lifetime for the totally constrained plate. Cracking of the beryllium cladding is predicted to occur under the more severe constraints, but the structural material should remain sound. The greatest uncertainty in the analysis is the bond between the coating and the structural material. Additional work is needed to evaluate off-normal events such as disruptions and loss-of-coolant accidents.

1.4 Tritium-Rich Startup Effects

During the startup of WILDCAT extra tritium was added to help heat the plasma to ignition and reduce the auxiliary power requirements. This procedure results in a peak in the thermal power that is 60% above the final, steady-state value and a peak in the wall loading that is over twice as large. There was concern that this extra power could reduce the wall and limiter lifetime.

Further study has shown that although the total wall load is substantially increased, the heat load on the wall is below its final value throughout the startup. Since it is this surface heat that produces the major stresses, it is concluded that no additional problems are encountered owing to this effect.

1.5 High-Field Magnet Support

Some further study of the support problem against out-of-plane loads for the toroidal field coils has been undertaken. WILDCAT has the major part of its overturning moment on the outer leg. The moment on the curved portion of the inner leg is in the opposite direction, and while this component of the moment tends to reduce the overall moment, the two components together act to twist the coil. The solution adopted is to use warm (room temperature) structural members, as opposed to cold supports, which require a complicated dewar. The support elements are epoxy-fiberglass tie bars connected to the vacuum tank at one side of the coil and to the helium vessel at the opposite side. This solution is not without problems which require further study.

The coil-to-coil support is provided by reinforced concrete consisting of three sectors between each coil. Only the middle sector needs to be removed for almost all access, and only a plug in the middle sector needs to be removed for the most frequently required access. Square keys provide alignment and transfer the shear. Each sector is entirely contained in a steel can with additional steel in high stress areas. This design is innovative and appears attractive. Sufficient effort has not been provided to fully assess its credibility.

1.6 Reactors with Less Than Full Tritium Breeding

The major effort of this report has been in the initial part of a study of reactors with a range of tritium concentrations ranging from a 50-50 D-T mixture as is typical of full D-T operation, for example, STARFIRE,[2] down to a low concentration corresponding to operation with no tritium breeding as is the case for WILDCAT. It is interesting to look at the reactor possibilities between these two extremes for several reasons, most importantly that full tritium breeding may not be possible, especially in near-term reactors. It is also possible that for some applications the best design might be an intermediate one. In addition, examination of the intermediate cases gives an indication of just where the beneficial features and disadvantages of each begin to occur, increasing the understanding of both the D-T and the D-D cases.

It is the purpose of this study to develop a sequence of reactor designs spanning the full range of tritium concentrations or, alternatively, tritium breeding ratios. The reactors are to be based as much as possible on STARFIRE and WILDCAT design philosophies, but a consistent set of parameters is assumed, in particular a fixed beta (10%), a fixed thermal power (4000 MWt) and fixed heat load on the first wall (1 MW/m^2). Optimum operating temperatures, sizes, toroidal field strengths, blanket/shield configurations, and detailed costs are to be determined for each case in order to investigate the advantages, disadvantages, and ramifications of tritium-depleted operation.

In this report a consistent set of assumptions is discussed and developed, the relationship between the tritium concentration and the required tritium breeding ratio is examined, the optimum operating temperature is determined along with the advisability of reinjecting ^3He, and some simplified cost issues are discussed. The full work will be published in a future report.[3]

The optimum temperature at which to operate a reactor is a somewhat sensitive and complicated function of the tritium concentration. This operating temperature has been taken to be the temperature for which the power density peaks or a few degrees above the minimum temperature for ignition, whichever is highest. The temperature ranges from 7 keV for the D-T case to 24 keV for the case where there is no tritium breeding. Three regimes appear. For tritium concentrations, r_T, greater that ~0.1 of the deuterium concentration or tritium breeding ratios, TBR, greater than ~94%, the reactors operate at the maximum power density without ^3He reinjection. For $r_T < \sim 0.01$ or TBR < ~40%,

reinjection of ^3He is necessary to obtain ignition, and operation is at a temperature a few degrees above the minimum temperature for ignition (in order to provide some margin of operation. The intermediate region with $0.1 < r_T < 0.01$ or 94% < TBR < 40% is a transition region.

A simple calculation of the increased cost of electricity due to operation at lower tritium levels indicates that tritium-depleted operation might be attractive if the cost of tritium were less than 2000 $/g. This value is substantially lower than today's prices; however, indications of the more detailed costing studies are that the above estimate may be too severe.

REFERENCES FOR CHAPTER 1

1. K. Evans, Jr., et al., "WILDCAT: A Catalyzed D-D Tokamak Reactor," ANL/FPP/TM-150, Argonne National Laboratory (1981).

2. C. C. Baker, et al., "STARFIRE - A Commercial Tokamak Fusion Power Plant Study," ANL/FPP-80-1, Argonne National Laboratory (1980).

3. K. Evans, Jr., J. G. Gilligan, and J. Jung, "Tokamak Fusion Reactors with Less Than Full Tritium Breeding, ANL/FPP/TM-169, Argonne National Laboratory (to be published).

Chapter 2

NON-MAXWELLIAN DISTRIBUTIONS

2. NON-MAXWELLIAN DISTRIBUTIONS

2.1 Introduction

The central defect characterizing advanced fuels is their low fusion cross sections, which also tend to peak at very high energies, compared to the D-T reaction. One figure of merit for fusion engineering is the local fusion power density, $n_i n_j \langle \sigma_{ij} v \rangle Q_{ij}$, where n_i is the density of species i, Q_{ij} is the energy released, σ_{ij} is the cross section for i-j fusion, and $\langle\ \rangle$ indicates a six-fold integral over velocity space. For magnetic confinement devices which are limited to a maximum plasma beta and magnetic field we convert fusion power density to a more useful form,

$$P_f = \frac{\beta^2 B^4}{T^2} \sum_{\text{reactions}} \langle \sigma_{ij} v \rangle$$

Unlike standard treatments of fusion reactions, we will consider non-Maxwellian velocity distributions of reactants, so beta, pressure, and temperature must be given more general definitions. We select a normalization such that

$$1 \equiv \int d^3v\ f_i(\underline{v}) \ ,$$

where $f_i(\underline{v})$ is the velocity distribution of the i-th species. Then, the pressure for the i-th species is defined in terms of the energy moment of f_i as

$$P_i = \frac{2}{3} n_i \int d^3v \frac{m_i v^2}{2} f_i(\underline{v}) \ ,$$

and the temperature is defined as $T_i = p_i/n_i$. The local plasma beta is defined as

$$\beta = \sum_i \frac{n_i T_i}{B^2/2\mu_0} \ ,$$

where B is the local magnetic field strength and n_i is the local density of the i-th species.

For fixed β and B we will endeavor to determine if the ratio $\langle\sigma_{ij}v\rangle T^{-2}$ can be increased for advanced fuels over the value for Maxwellian reactants by suitable modifications to the distribution functions. In particular, we will study tail elevation of $f(\underline{v})$ via ion cyclotron resonant heating (ICRH). We note that σ_{ij} for the common D-D reactions rises very quickly at high energies (~100 keV) so small increases in the ion tail population may significantly increase $\langle\sigma_{ij}v\rangle$ without appreciably increasing T, since the temperature is a strong function of the thermal population alone. One caution must be observed. The bulk of magnetic confinement stability theory deals with plasmas with Maxwell-Boltzmann velocity distributions. To the extent that ICRH significantly destroys the Maxwellian nature of $f(\underline{v})$ the upper limit on β may be likewise changed. Any results calculated here must be of moot significance until it is known whether β increases or decreases under the influence of ICRH.

Numerous precedents exist for calculations of non-Maxwellian fusion reaction rates. Tail depletion has been studied as a concern for inertial fusion,[1] since high energy ions are most easily lost from small imploding pellets. Tail modification has been studied for advanced fuels with regard to the effects of nuclear elastic scattering.[2] Tail elevation by neutral beam injection has been studied for advanced fuels[3] and is essential to the successful demonstration of D-T fusion in small devices such as TFTR.[4]

Our study has been motivated by the experimental verification of the ICRH theory[5] at moderate power levels on such tokamaks as PLT. Charge-exchange diagnostics indicate $f(\underline{v})$ is in close agreement with the theoretical values for both minority fundamental heating[6] and majority harmonic heating.[7] Our calculations presume that ICRH may be employed during reactor operation in a steady-state mode, and we must ultimately question whether $\langle\sigma v\rangle/T^2$ can be increased enough so that the increased fusion power offsets the rf input power to the plasma.

2.2 Calculations

The present work concerns only fundamental ICRH, for which Stix[5] provides analytic solutions to the quasilinear-Fokker Planck equation. Stix assumes a small number of high energy ions are resonant with the fast wave and allows them to thermalize against electrons and background ions (which may be thermal

energy ions of the same species.) We use a distribution function which assumes an isotropic velocity space distribution. This assumption, expected to be good except at very high energies, has been shown to be very accurate, according to the PLT data.[6] In terms of the ion energy, E, the distribution function is given by

$$\ell n\ f(E) \;=\; \frac{-E}{(1+\xi)T_e}\left\{1 + \frac{R_i\left(T_e - T_b + \xi T_e\right)H}{T_b\left(1+\xi+R_i\right)}\right\}$$

with

$$H\left(x = E/E_i\right) \;\equiv\; \frac{1}{x}\int_0^x \frac{du}{1+u^{3/2}}$$

$$= \frac{2}{x}\left\{\frac{1}{6}\,\ell n\left[\frac{1-\sqrt{x}+x}{1+2\sqrt{x}+x}\right] + \frac{1}{\sqrt{3}}\left[\frac{\pi}{6} + \tan^{-1}\frac{2\sqrt{x}-1}{\sqrt{3}}\right]\right\}.$$

Here T_e is the electron temperature, T_b is the background ion temperature

$$T_b \;\approx\; \lim_{E\to 0}\left(-d\ \ell n\ f/dE\right)^{-1},$$

ξ is a parameter relating the ICRH power density, $R_i = Z_{eff}\left(3m_bT_e/m_eT_b\right)^{1/2}$, m_b and m_e are the field ion and electron masses, Z_{eff} is an <u>ad hoc</u> generalization of Stix's single field ion expression to multiple species,

$$Z_{eff} \;=\; \sum_j \frac{n_j Z_j^2}{n_e},$$

n_j and n_e are the ion and electron densities, Z_j is the charge of the j-th ion species and

$$E_i \;=\; \left(m_iT_b/m_b\right)\left[\left(1+\xi+R_i\right)\times 1.33/(1+\xi)\right]^{2/3},$$

where m_i is the (test) ion mass undergoing ICRH. When E is expressed in units of keV the temperature is

$$T_i = 2.402 \times 10^{-23} m_i^{-3/2} N \int_0^\infty dE\, E^{3/2} f(E) .$$

We specialize our investigation to fundamental ICRH of a plasma with a single ion species, deuterium, so $m_b = m_i$. Figure 2-1 displays f(E) for ξ = 10, with Z_{eff} = 1.5, T_e = 15 keV, and T_D = 12.76 keV. It is apparent that ICRH results in tail elevation, as desired.

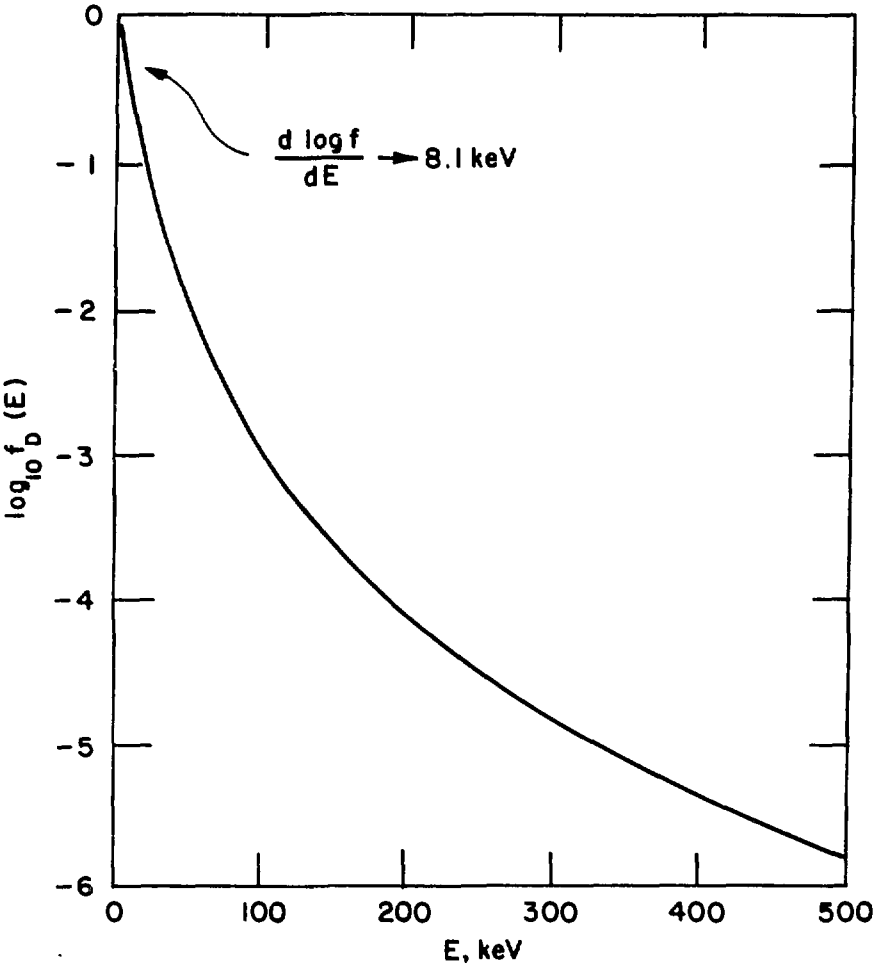

Fig. 2-1. Fundamental (n = 1) majority D heating results in non-Maxwellian $f_D(\varepsilon)$ [Stix, Nucl. Fusion 15, 73 (1975)]. Example below is for Z_{eff} = 1.5, T_e = 15 keV, ξ = 10. The effective "temperature" is T_D = 12.76 keV.

For unlike ion species the differential reactivity for all of species 2 to fuse with a phase space element of species 1 of volume d^3v_1 is

$$d\langle\sigma_{12}v\rangle = \left\{\int d^3v_2 f_2(\underline{v}_2)\sigma_{12}(|\underline{v}_1 - \underline{v}_2|)|\underline{v}_1 - \underline{v}|\right\} f_1(\underline{v}_1)\, d^3\underline{v}_1$$

$$= f_1(\underline{v}_1)\, d^3v_1 \int_0^{2\pi} d\phi \int_0^{\pi} d\theta \int_0^{\infty} dv_2 v_2^2 \sin\theta\, f_2(\underline{v}_2)\sigma_{12}(V)V \ ,$$

where

$$V \equiv |\underline{v}_1 - \underline{v}_2| = \sqrt{v_1^2 + v_2^2 - 2v_1v_2\cos\theta} \ ,$$

and θ is the angle between $\underline{v}_1$ and $\underline{v}_2$. For the case of interest, isotropic distribution functions, this integral simplifies considerably:

$$d\langle\sigma_{12}v\rangle = f_1(v_1)\, d^3v_1\, 2\pi \int_0^{\pi} d\theta \int_0^{\infty} dv_2 v_2^2 \sin\theta\, f_2(v_2)\sigma_{12}(V)V$$

$$= -f_2(v_1)d^3v_1\, 2\pi \int_0^{\infty} dv_2 v_2^2\, f_2(v_2) \int_1^{-1} d(\cos\theta)\sigma_{12}[V(\cos\theta)]V(\cos\theta)$$

$$= \frac{f_1(v_1)\, d^3v_1}{v_1} \int_0^{\infty} dv_2 \frac{v_2^2 f_2(v_2)}{v_2} \int_{|v_2-v_1|}^{|v_2+v_1|} dV\, V^2\sigma_{12}(V) \ .$$

For like particle (D-D) reactions, we reduce this expression by a factor of two and perform the integral over all of phase space:

$$\frac{1}{2}\langle\sigma_{DD}v\rangle = 4\pi^2 \int_0^{\infty} dv_1\, v_1 f(v_1) \int_0^{\infty} dv\ {}_2v_2 f(v_2) \int_{|v_2-b_1|}^{|v_2+v_1|} dV\, v^2\sigma_{DD}(V)$$

where $v_{1,2} \equiv |\underline{v}_{1,2}|$. Finally, changing variables from speed to energy (in keV),

$$\langle\sigma_{DD}v\rangle = 6.1058 \times 10^{40}\, A\, m_D(\text{amu})^{-7/2} \int_0^{\infty} \int_0^{\infty} dE_1\, dE_2\, f(E_1)f(E_2)I \ ,$$

where

$$I(E_1,E_2) = \int_{E_\ell^{1/2}}^{E_u^{1/2}} dx \, \frac{\left[e^{B/x} - 1\right]^{-1}}{\left[1 + (C - Dx^2)^2\right]} ,$$

with $E_\ell^{1/2} \equiv \left|E_1^{1/2} - E_2^{1/2}\right|$ and $E_u^{1/2} \equiv E_1^{1/2} + E_2^{1/2}$. In terms of this expression for $\langle\sigma_{DD}v\rangle$ the local D-D fusion reaction rate is $1/2\ n_D^2\langle\sigma_{DD}v\rangle$.

In obtaining this result we have followed the standard approach of fitting $\sigma(E)$ data with an analytic curve:

$$\sigma(E) = A\,E^{-1}\left[1 + (C - DE)^2\right]^{-1}\left[e^{B/E^{1/2}} - 1\right]^{-1} .$$

The values of the four constants are given in Table 2-1 for the two branches of the D-D reaction. The reader is cautioned that there are grievous errors in previously published values of these constants appearing in two widely distributed documents, Refs. 8 and 9.

Table 2-1. Analytic Function for D-D Fusion Cross Section: $\sigma(E) = AE^{-1}\left[1 + (C - DE)^2\right]^{-1}\left[\exp\left(B/\sqrt{E}\right) - 1\right]^{-1}$

Constant	D + D → T + p	D + D → ^{3}He + n
A	372 keV-barn	482 keV-barn
B	46.097 $keV^{1/2}$	47.88 $keV^{1/2}$
C	1.220	1.177
D	4.36×10^{-4} keV^{-1}	3.08×10^{-4} keV^{-1}

Numerical calculations of $\langle\sigma_{DD}v\rangle$ were performed for the ^{3}He branch to gauge the impact of ICRH on D-D fusion reaction rates. Figure 2-2 displays the relevant parameter $\langle\sigma_{DD}v\rangle T_D^{-2}$ for T_b = 5 keV at various ξ and three values of T_e. In the Maxwellian limit, $\xi \ll 1$, $\langle\sigma v\rangle$ is, of course, independent of T_e. As ICRH becomes stronger the deuterons' slowing down is mostly determined at high energies by the electron drag,[5] so a disparity in the $\langle\sigma v\rangle T_D^{-2}$ develops for different T_e values. Notice $\langle\sigma_{DD}v\rangle T_D^{-2}$ increases initially at small values of ξ, due to the increase in $\langle\sigma_{DD}v\rangle$. However, at high heating levels the

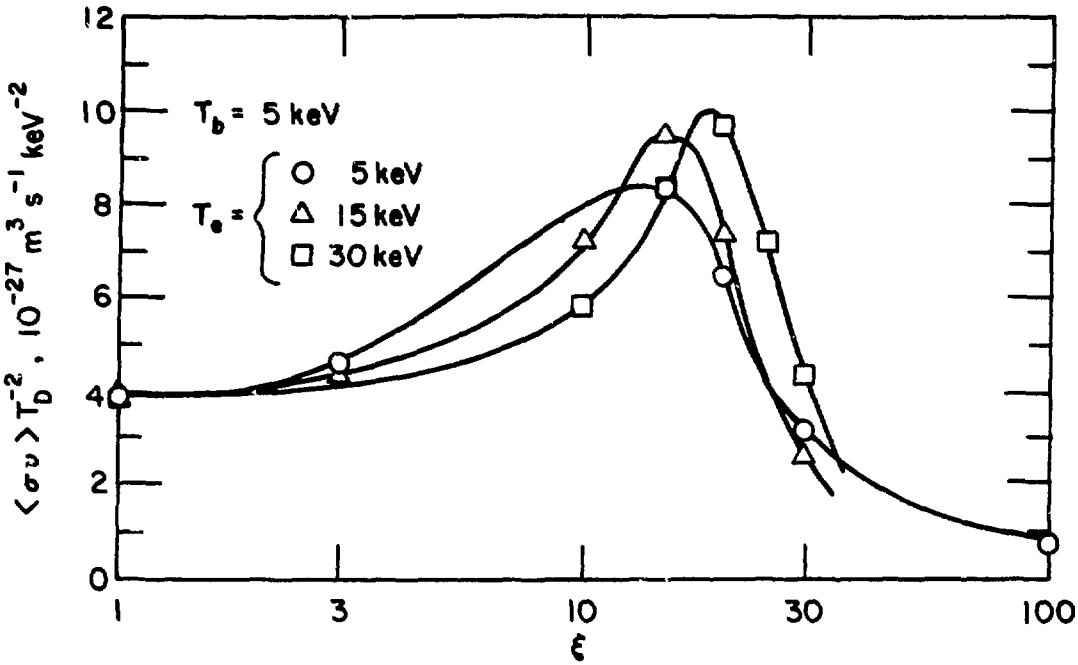

Fig. 2-2. Reaction rate versus ICRH power density.

$f_D(v)$ distribution gets so severely distorted in the thermal region that T_D^2 increases faster than $\langle\sigma_{DD}v\rangle$.

We note that plasma transport theory generally deals with ions which are assumed to be approximately Maxwellian. Hence, it is not evident how to use the T_D parameter in fusion reactor calculations when f_D is not Maxwellian. Nevertheless, we have also tabulated $\langle\sigma_{DD}v\rangle T_D^{-2}$ as a function of T_D, and a selection of results is plotted in Fig. 2-3. The result labeled $\xi = 0$ is the usual curve[9] utilized for advanced fuel studies. With the addition of fundamental ICRH with $\xi = 10$ we find significant increases in $\langle\sigma_{DD}v\rangle T_D^{-2}$, the exact value depending on T_e. The best case so far, with $\xi = 20$, $T_e = 30$ keV, and $T_D = 13.5$ keV, has $\langle\sigma_{DD}v\rangle T_D^{-2}$ 40% larger than the best value for Maxwellian distributions.

2.3 Future Work

The investigation of fundamental ICRH has not been pursued any further for a number of reasons. In the first place, we would like to find an order of magnitude increase in $\langle\sigma_{DD}v\rangle T_D^{-2}$ rather than a few percent, due to the

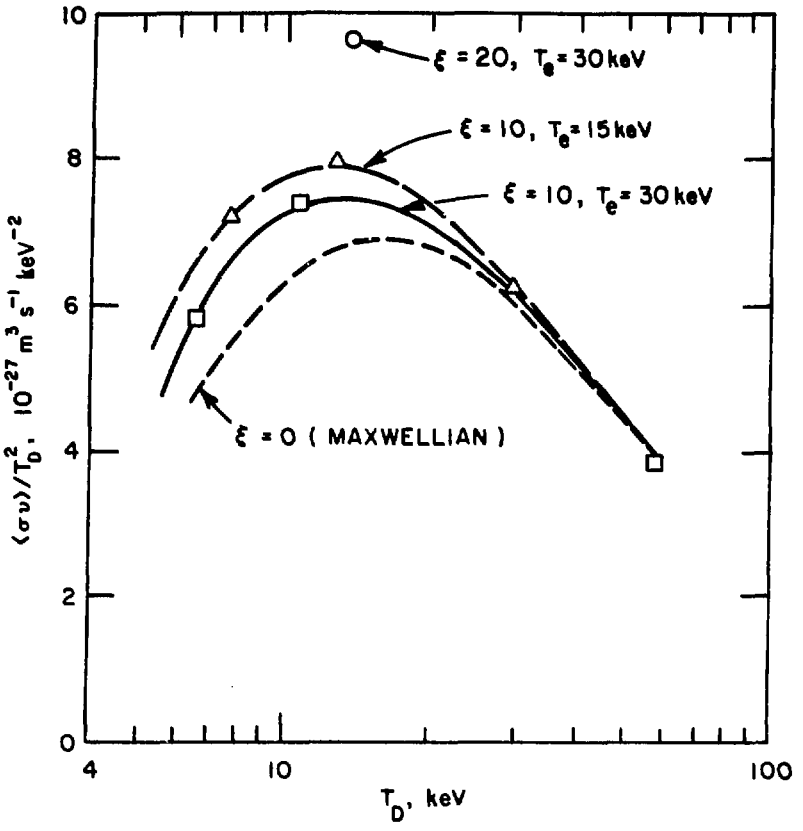

Fig. 2-3. Enhanced fusion reactivity, $\langle\sigma_{DD}v\rangle/\tilde{T}_D^2$, for DD → n^3He from fundamental (n = 1) majority heating. [Best case so far: $\langle\sigma_{DD}v\rangle/\tilde{T}^2 = 9.7 \times 10^{-27}$ m^3s^{-1} keV^{-2} at $\xi = 20$, $T_e = 30$ keV, $\tilde{T}_D = 13.5$ keV.]

fact that advanced fuel reaction rates are orders of magnitude lower than D-T values. Moreover, these small increases in $\langle\sigma_{DD}v\rangle T_D^{-2}$ do not seem large enough to offset the rf power invested to create the tail distortion. Following Stix[5] we relate ξ to the rf power density, $\langle P\rangle$, as

$$\xi = 4.16 \times 10^{34}\, m_D T_e^{1/2} \left(n_D n_e \ell n \Lambda Z_D^2\right)^{-1} \langle P\rangle ,$$

where $\ell n \Lambda$ is the usual Coulomb logarithm. Figure 2-4 displays $\xi(r)$ for WILDCAT with 100 MW of ICRH absorbed in the plasma, using an approximate model for the spatial profile of $\langle P\rangle$. We see $\xi \lesssim 0.02$ where $T_D \approx 10$-20 keV. Now, 100 MW invested in the plasma could require 150 MW of electric power to the rf

system. To break even, this in turn would require an increase of the reactor's thermal power by about 450 MW, representing a 15% increase in the value of $\langle\sigma_{DD}v\rangle T_D^{-2}$, averaged over the plasma. Reference to Fig. 2-3 demonstrates that $\xi \gtrsim 10$ is needed to accomplish this in the plasma periphery where $T_D \lesssim 30$ keV, while $\xi >> 10$ is needed in the high-temperature interior. Figure 2-4 shows that this is not achieved.

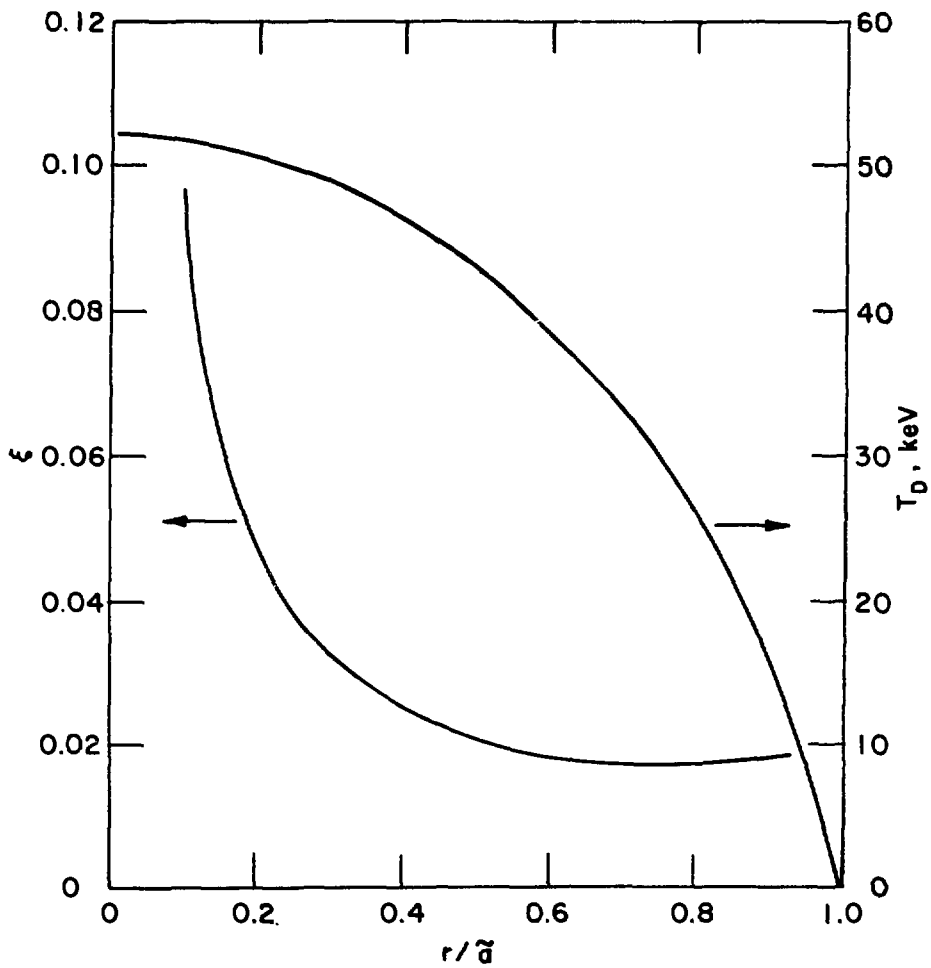

Fig. 2-4. For 100 MW of auxiliary heating at the fundamental, the benefits are negligible since $\xi(r)$ is so small in the regions where T_D is in the range 10-20 keV.

Harmonic ICRH may well be a more interesting technique for advanced fuels. The higher frequencies present easier reactor engineering prospects since waveguide couplers become more realistic above 100 MHz.[10] More importantly, harmonic ICRH has a Larmor radius dependence to the quasilinear diffusion coefficient[11] which may promote tail elevation at relatively high

energies resulting in significantly higher $\langle\sigma_{DD}v\rangle T_D^2$ values than fundamental heating. (In addition, we note fundamental ICRH of the majority species may be difficult to achieve in toroidal plasmas since the fast wave polarization may couple to minority ion hybrid resonances).

Therefore, we infer that the most fruitful course of study would be harmonic ICRH. Fokker-Planck-quasilinear codes are now available to numerically compute $f_D(v)$ from any ICRH harmonic, assuming only isotropy in phase space. These routines are fully coupled to toroidal ray tracing programs such that realistic spatial profiles for $f_D(v)$ can be calculated. In closing we mention that ICRH might be employed as well for other purposes such as toroidal current maintenances (although only minority ICRH has been studied to date). In this sense the rf power investment may have multiple benefits to tokamak operations.

REFERENCES FOR CHAPTER 2

1. A. G. Petschek, D. B. Henderson, Nucl. Fusion 19, 1678 (1979).
2. J. Galambos, et al., Annual Controlled Fusion (Sherwood) Theory Conference, 1981, Austin, Texas, paper 1C34.
3. C. Bathke, H. Towner, and G. H. Miley, Trans. Am. Nucl. Soc. 17, 41 (1973).
4. D. J. Jassby, Nucl. Fusion 17, 309 (1977).
5. T. Stix, Nucl. Fusion 15, 737 (1975).
6. J. Hosea, et al., Phys. Rev. Lett. 43, 1802 (1979).
7. J. Hosea, et al., in Proc. Conf. on Plasma Physics and Controlled Nuclear Fusion 1980 (IAEA, VIENNA, 1981), Vol. II, p. 95.
8. D. L. Book, Naval Research Laboratory Memorandum Report 3332, p. 77 (1977).
9. G. H. Miley, H. Towner, and N. Ivich, "Fusion Cross Sections and Reactivities," COO-22188-17, University of Illinois (1974)
10. F. W. Perkins, Bull. Am. Phys. Soc. 26, 929 (1981).
11. C. F. F. Karney, Princeton Plasma Physics Laboratory, private communication (1981).

Chapter 3

HELIUM-3 PRODUCING BLANKET

3. HELIUM-3 PRODUCING BLANKET

The possibility of breeding ^3He in a blanket of a fusion reactor has been considered as a possible source of ^3He for the D^{3}He fusion reactors. A survey of the nuclear data was conducted to define elements with (n,^{3}He) reaction cross sections. The data libraries[1,2] based on the Evaluated Nuclear Data File (ENDF) and the Evaluated Nuclear Data Library (ENDL) were searched for that purpose. Table 3-1 lists the materials with (n,^{3}He) reaction cross sections at neutron energies of 14 MeV, reaction Q values and the year of publication. The existing data for the (n,^{3}He) reaction cross section values vary from a few μb to 8 mb. These small values are related to the high negative reaction Q values. At neutron energies of 14-MeV, the ^3He ions have energies below Coulomb barrier for almost all (n,^{3}He) reactions due to the high negative Q values. This is one of the main reasons for the low (n,^{3}He) reaction cross sections. Calcium has the highest cross section relative to the other elements in Table 3-1. However, Table 3-2 shows that Ca(n,^{3}He) reaction cross section is very small relative to the total cross section; it is less than 0.4% of the total cross section.

A neutron transport calculation in a calcium medium was performed to determine the main reaction rates per fusion neutron. A calcium sphere with a 100-cm radius and a 14-MeV neutron source located at the center were used for the calculations. The results show a high neutron leakage rate of 0.53 per fusion neutron because calcium has a very low radioactive capture cross section. The ^3He production rate is 0.0054 atom per fusion neutron which is quite small relative to the hydrogen and ^4He production rates as shown in Table 3-3. In addition, the ^3He cross section is quite large, that is the reaction $^3He(n,p)T$ has a value of $\sim 10^4$ barns for thermal neutrons. For a calcium blanket with a low absorption, a large fraction of ^3He produced will interact with thermal neutrons generating tritium. This leads us to conclude that it is not practical to produce the ^3He in a fusion blanket based on the existing nuclear data.

Table 3-1. Elements with (n,^{3}He) Cross Section

Element	Energy (MeV)	(n,^{3}He) (μb)	Reaction Q Value (MeV)	Year of Publication
$_{13}Al^{27}$	14.8	0.500	-14.70	1960
$_{15}P^{31}$	14.0	0.222	-13.08	1971
	14.8	0.700		1960
$_{19}K^{41}$	14.0	0.848	-12.61	1971
$_{20}Ca$	14.0	7.313	-6.99[a]	1974
	14.8	7.560		1974
$_{25}Mn^{55}$	14.0	0.800	-12.70	1971
	14.8	4.000		1960
$_{27}Co^{59}$	14.0	0.062	-11.61	1971
	14.8	2.000		1960
	14.8	0.017		1965
$_{29}Cu^{63}$	14.0	0.113	-9.51	1971
	14.1	3.000		1961
$_{29}Cu^{65}$	14.8	4.000	-12.21	1960
$_{31}Ga^{71}$	14.0	0.066	-11.04	1971
$_{33}As^{75}$	14.0	0.578	-10.15	1971
	14.8	5.000		1960
	14.8	0.500		1965
$_{40}Zr^{96}$	14.0	0.136	-13.47	1971
$_{41}Nb^{93}$	14.0	0.018	-7.71	1971
$_{45}Rh^{103}$	14.0	0.016	-8.55	1971
	14.7	0.001		1966
	14.8	2.500		1960
	14.8	0.013		1963
	14.8	0.002		1968
$_{47}Ag^{109}$	14.0	0.023	-8.72	1971
$_{49}In^{115}$	14.0	0.033	-9.36	1971
$_{52}Te^{130}$	14.0	0.015	-10.80	1971
$_{55}Cs^{133}$	14.7	0.005	-7.58	1965
$_{75}Re^{187}$	14.0	0.006	-6.6	1971

[a]This Q value for $_{20}Ca^{40}$ isotope.

Table 3-2. Ca(n,^{3}He) and Total Cross Section as a Function of the Neutron Energy

Energy (MeV)	(n,^{3}He) (μb)	Total Cross Section (μb)
10.4	0.[illegible]1	2502.0
11.0	0.10	2459.0
11.6	1.00	2390.0
12.0	2.70	2355.0
12.4	4.65	2304.0
12.8	5.85	2244.0
13.2	6.50	2246.0
13.6	6.95	2195.0
14.0	7.30	2149.0
15.0	7.60	2117.0

Table 3-3. Main Nuclear Reactron Rates per Fusion Neutron in a Calcium Medium

Reaction Rate	Value
(n,α)	0.1568
(n,^{3}He)	0.0054
(n,D)	0.0139
(n,p)	0.2847
(n,γ)	0.0032
Leakage	0.5282
Total hydrogen production	0.7359
Total helium production	0.2303

REFERENCES FOR CHAPTER 3

1. O. E. Cullen, R. J. Howerton, M. M. MacGregor, and S. T. Perkins, "An Integrated System for Production of Neutronics and Photonics Calculational Constants, Supplemental Neutron-Induced Interactions," UCRL-50400, Lawrence Livermore Laboratory (1976), Vol. 8, Rev. 1, Pts. A and B.

2. Y. Gohar and M. A. Abdou,. "MACKLIB-IV: A Library of Nuclear Reponse Functions Generated with MACK-IV Computer Program from ENDF/B-IV," ANL/FPP/TM-106, Argonne National Laboratory (1978).

Chapter 4

MATERIALS ANALYSIS

4. MATERIALS ANALYSIS

The materials analysis for WILDCAT for FY 1982 has consisted of upgrading the one-dimensional lifetime code to accommodate a dual material configuration; e.g. beryllium on stainless steel, graphite on copper, etc. This section presents first a summary of the code capabilities and then presents the upgraded results of the analysis of the WILDCAT first wall. A detailed description of the code is given elsewhere.[1]

4.1 Lifetime Code Description

The flow diagram for the lifetime code is shown in Fig. 4-1. The code first calculates the temperature, stress, and strain distributions through a plate based upon the selected operating and design parameters. Property changes are then determined for a specific time increment, and the effects of those changes on the initial distributions are evaluated. This process is repeated until failure occurs or the desired lifetime is reached.

The basic inputs to the code are the operating and design parameters. The design parameters include component material(s) selection, plate thickness, coolant characteristics, primary stress level, initial crack length, and plate constraint. The operating parameters include the burn cycle characteristics (ramp time, burn time, dwell time), down period duration and frequency surface heat flux, neutron wall loading, and surface erosion rate. Finally, the failure criteria for swelling, deformation, and ductility are also provided.

Either a single or dual material plate can be analyzed by the code. The dual material plate is representative of components which are likely to have a low-Z material bonded to a structural material. The materials properties which are considered are the thermophysical, mechanical, swelling, and neutronic properties as shown in Table 4-1. Temperature is the primary parameter considered for the thermophysical properties. Radiation effects are also considered in the cases of the thermal conductivity and the elastic modulus. The mechanical properties considered are the tensile, crack growth, fatigue, and creep properties. A bilinear elastic-plastic behavior is assumed for the tensile properties. Temperature, stress, fluence, stress and strain ranges, and

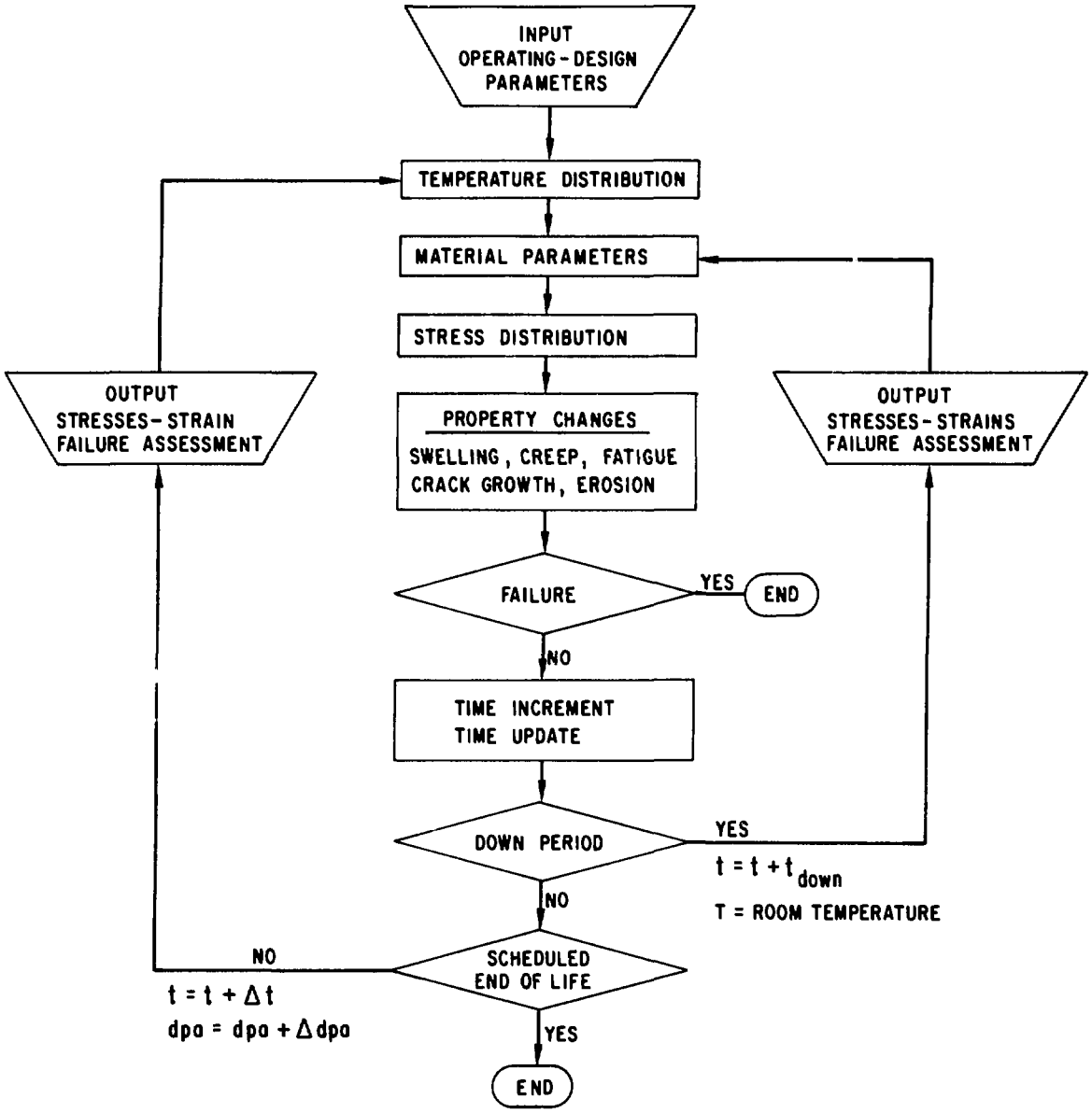

Fig. 4-1. Lifetime code flow diagram.

Table 4-1. Properties Considered in Lifetime Analysis

Property	Parameters
Thermal conductivity	Temperature, fluence
Specific heat	Temperature
Density	Temperature
Thermal expansion	Temperature, fluence
Young's modulus	Temperature, fluence
Poisson's ratio	Temperature
Uniform elongation	Temperature, fluence
Yield stength	Temperature, fluence
Ultimate tensile strength	Temperature, fluence
Crack growth	Stress intensity, temperature, stress ratio
Fatigue	Strain range, temperature, fluence, average stress
Creep	Stress, temperature, fluence
Swelling	Temperature, fluence
Nuclear heating	Flux
Helium production	Fluence
dpa	Fluence

stress intensity are the parameters included in determining the mechanical properties. Radiation swelling is dependent on the temperature and fluence, and the neutronic properties depend on the neutron flux and fluence.

A simple thermal-hydraulics subroutine calculates the temperature distribution through the plate at various times during the burn cycle. The temperature distribution is then used to calculate the thermal strain distribution, which is used as input to calculate the stress distribution. The stresses can be determined for a plate which is either totally constrained from expansion, allowed to expand but not bend, or unconstrained. These three conditions span the possible range of component constraint in the reactor.

Once the temperature, stress, and strain distributions are determined, the long-term response of the material to the reactor environment can be evaluated. The code determines the swelling change, creep change, fatigue damage, and crack growth for a time increment Δt. The swelling and creep

which occurs during the period Δt results in a modified strain distribution that is used to calculate the changes in the stresses. The code also determines the amount of surface erosion during the time increment. The reduction in plate thickness results in a modified temperature distribution. The property change calculations are then repeated using the modified distributions until either a failure criteria is met or the component reaches the goal lifetime. For calculational purposes the temperature and stresses are assumed to remain constant during the time increment. Therefore, Δt must be chosen such that the stress change is small compared with the total stress in order for this approach to reasonably approximate reactor behavior.

4.2. First Wall Response

The first wall design is unchanged from last year. A schematic of the first wall which utilizes a coolant panel concept is shown in Fig. 4-2. The panels are made of PCA stainless steel and consist of a 1.5-mm thick corrugated sheet attached to a backplate which is 3 mm thick. The light-water coolant flows in the closed parts of the corrugation. The center-to-center distance between the coolant channels is 19 mm and the cross-sectional area of the coolant channels is 35% of the volume of the first wall. The corrugated part of the coolant panels has a low-Z coating consisting of 3 mm of beryllium. The coolant panels are attached to monolithic blanket blocks. The coolant fraction for the blanket region is 10% on the average, the balance being PCA stainless steel.

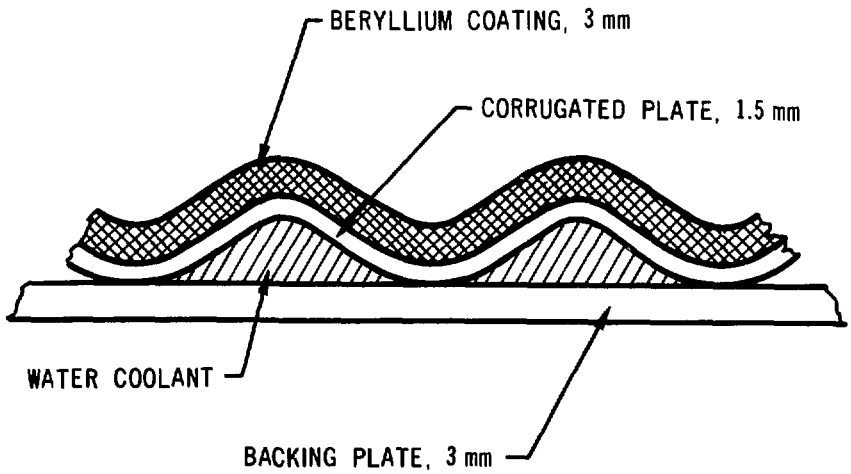

Fig. 4-2. Schematic cross section of first wall.

The lifetime of the first wall in WILDCAT has been estimated with the one-dimensional computer code described above. The reactor conditions used for the calculations are given in Table 4-2. The first wall configuration represents the outer part of the corrugations and is assumed to be a plate that receives uniform surface heat and neutron fluxes. The outer 3 mm of the plate, which faces the plasma, is beryllium, and the remaining 1.5 mm is PCA, an austenitic stainless steel that is very similar to Type 316 stainless steel. The primary differences between the two steels are the lower swelling and creep rates predicted for PCA. The STARFIRE first-wall structural material is also PCA and additional property data are given in that report.[2] The sputtering loss rate of the first wall has been determined assuming the sputtering characteristics of beryllium. The beryllium is assumed to be 70% of the theoretical density in order to accommodate the helium generated by neutron irradiation. The reduced density results in a lower thermal conductivity, however. Two constraints on the plate have been analyzed. The plate is assumed to be either totally constrained or allowed to expand but not bend. These conditions are believed to span the possible range of constraints for the first wall.

The sputtering rate of the first wall has been determined using the particle flux parameters shown in Table 4-2. All ionized particles coming out of the plasma are expected to strike the limiter so that only charge exchange neutrals strike the first wall. Since the helium and beryllium particles are predicted to remain in the ionized state, they do not strike the first wall. The particle energy distribution is assumed to be a Maxwellian that is peaked at 1200 eV. This energy is considerably above the energy (~400 eV) for peak sputtering for beryllium, and therefore the sputtering loss rate is quite low. The model used to determine the sputtering rate is that developed by Smith.[3,4] The physical sputtering coefficient is calculated to be 0.0105 and results in a calculated sputtering loss rate of 1.45×10^{-4} m/y at a 100% duty factor.

The temperature distribution through the first wall at several times during the reactor lifetime is shown in Fig 4-3. The surface of the plate exposed to the plasma for this and all other relevant figures in this section is the zero point of the abcissa. The figure indicates that the temperature gradient is reduced in the beryllium because of its high thermal conductivity compared to PCA. Perfect thermal contact is assumed between the two materials so that

Table 4-2. First-Wall Parameters for Lifetime Calculations

Operating Parameters	
Surface heat flux, MW/m^2	1.13
Neutron wall load, MW/m^2	0.6
Surface particle flux, $(n/m^2)/s$	3.72×10^{19}
Particle flux composition, %	
Hydrogen	6.6
Deuterium	93
Tritium	0.4
Average particle energy, eV	1200
Burn time - steady-state case, mo	6
Design Parameters	
Plate thickness, mm	
PCA	1.5
Beryllium	3
Coolant inlet temperature, °K	553
Heat transfer coefficient, $(W/m^2)/K$	20,000
Plate constraint	Free to expand, but not bend. Totally constrained.
Initial crack length, mm	0
Material Parameters	
Material	
Structure	PCA
Surface	Beryllium
dpa rate, $dpa/(MW\text{-}y/m^2)$	17.7
Helium generation rate, $appm/(MW\text{-}y/m^2)$	125

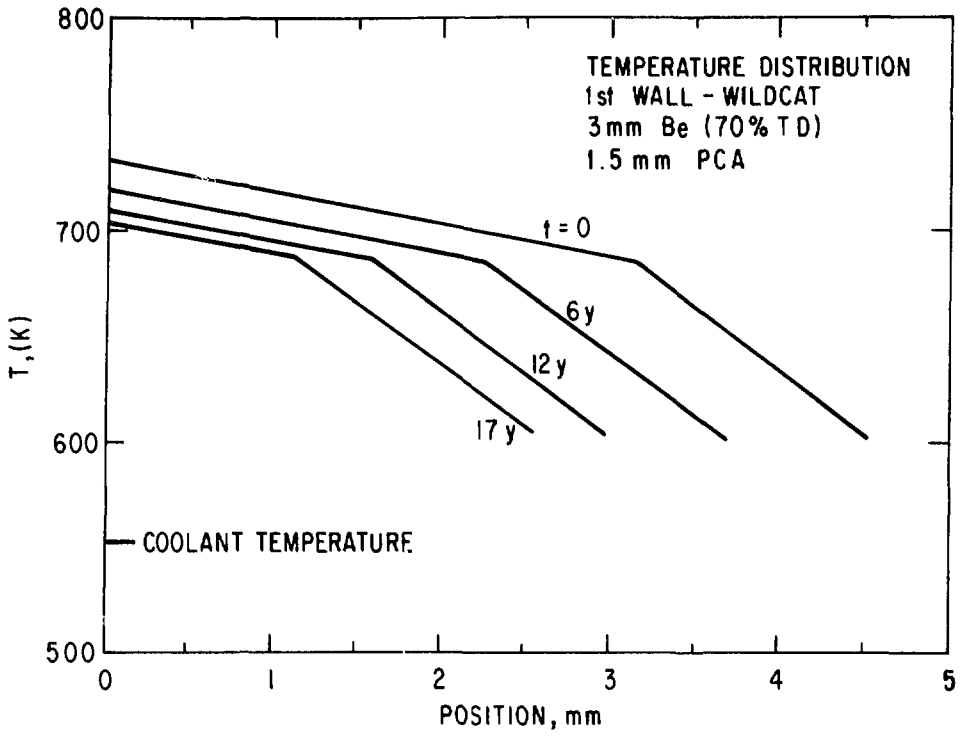

Fig. 4-3. Temperature distribution through the beryllium-PCA first wall at several times during the reactor history.

there is no temperature drop at the interface. The beryllium surface temperature is 735K at the start of the reactor life, and it drops down to ~700K at the end of 20 y as the surface is eroded. This compares with a temperature of 835K for a 4.6-mm thick first wall composed entirely of PCA.[5]

The thermal gradients through the plate are largely responsible for the generation of the operating stresses. The stress distributions through the plate for the two plate constraints are shown in Figs. 4-4 and 4-5. In the case of the plate which is allowed to expand but not bend (Fig. 4-4), the stresses remain below the yield stress for both beryllium and PCA. (Negative stresses are compressive and positive stresses are tensile.) The changes in stress with time are due primarily to radiation creep which tends to reduce the stress during the burn cycle and increase the stress during the off cycle. The calculated stresses are relatively low in this case, and no failures are predicted during the 20-y lifetime of the first wall.

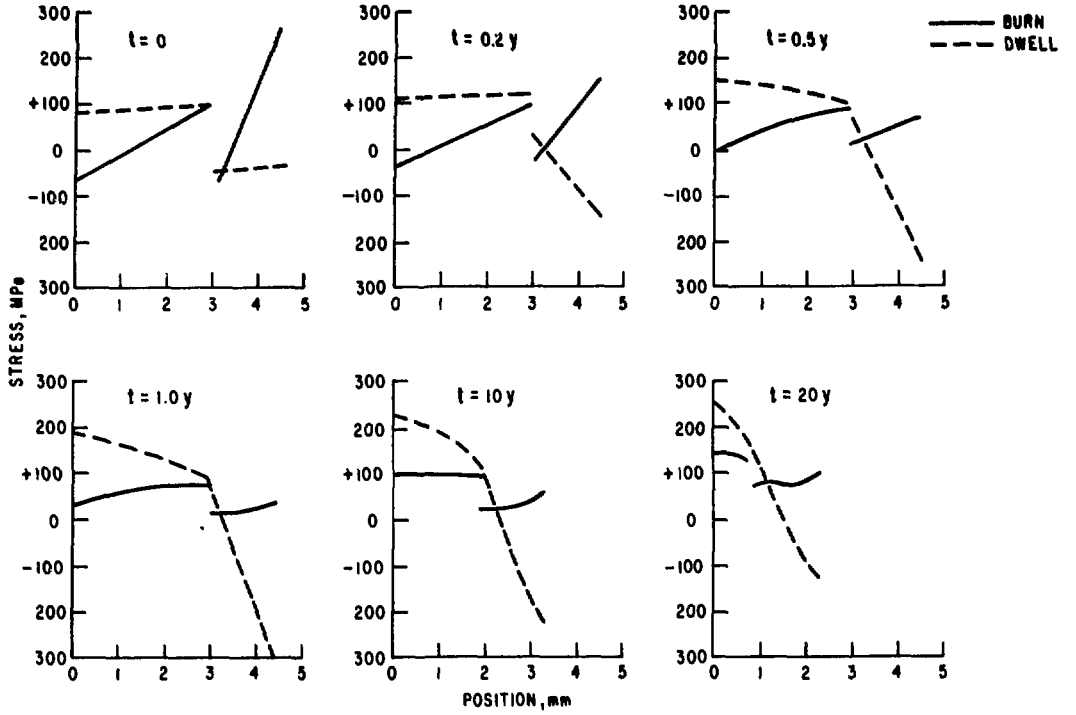

Fig. 4-4. Stress distribution through the beryllium-PCA first wall at several times for a plate that is allowed to expand but not bend.

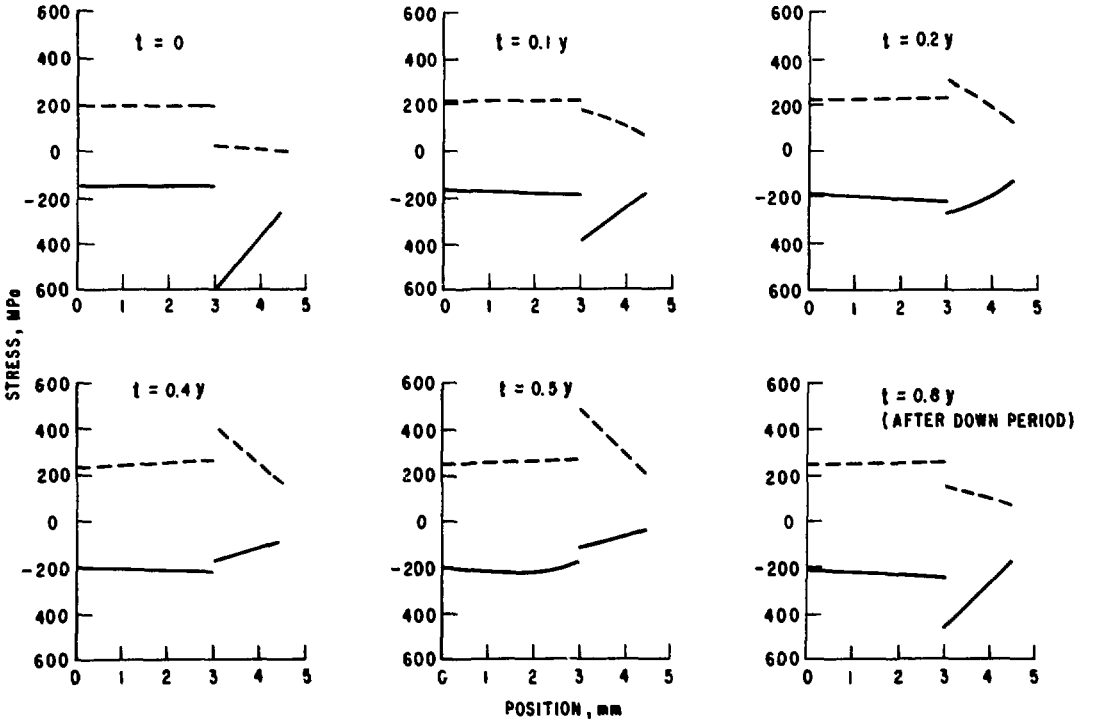

Fig. 4-5. Stress distribution through the beryllium-PCA first wall at several times for a plate that is totally constrained.

The results of the totally constrained case are shown in Fig. 4-5. The PCA stresses are still below the yield strength, but the stresses in beryllium exceed the yield strength, resulting in plastic deformation. The beryllium yield strength is, in fact, exceeded during both the burn cycle and the off cycle over most of the 20-y lifetime. The greater amount of strain compared with the previous case is predicted to lead to cracking of the beryllium layer, although no cracking is predicted to occur in PCA. Cracking of the surface layer only is not believed to a problem. Down periods are predicted to alter the stress distribution in the totally constrained case due to additional plastic strain caused by the reduction in temperature during the shutdown period. The stress distribution following shutdown is similar to the stress distribution at the start of the reactor life. In spite of the higher stresses and strains, a totally constrained plate is predicted to meet the 20-y lifetime.

Radiation causes changes in the tensile properties of beryllium and PCA as shown in Figs. 4-6 and 4-7. In general, the strength increases and the

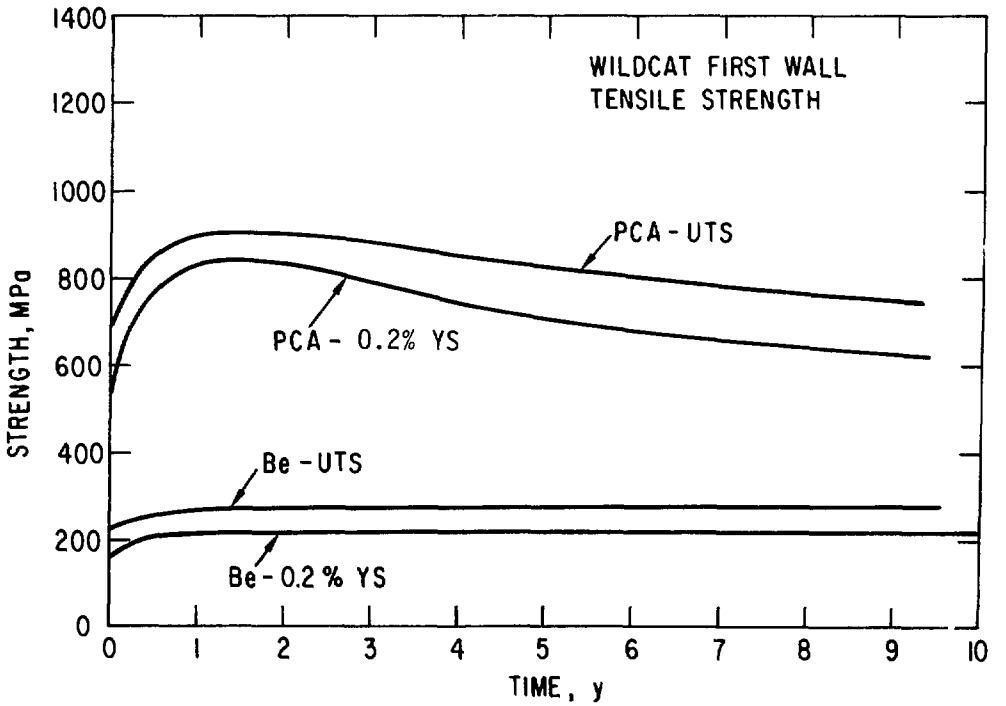

Fig. 4-6. Predicted change in beryllium and PCA tensile strengths as a function of time.

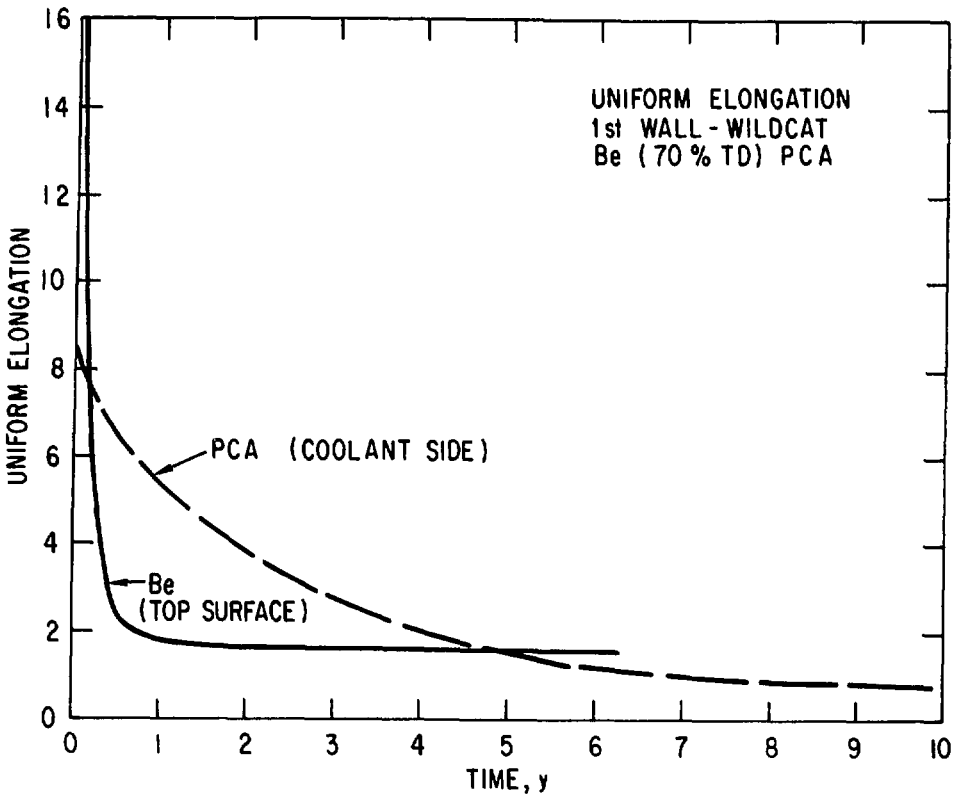

Fig. 4-7. Predicted change in beryllium and PCA uniform elongation as a function of time.

ductility decreases with neutron fluence. PCA is stronger than beryllium, and the loss of ductility occurs at a lower rate in PCA. During normal operation, the loss of ductility is not predicted to result in failure of the first wall, but off-normal events could lead to brittle failure. The total amount of swelling and creep is calculated to be <1%, which has a minimal effect on lifetime.

In conclusion, for normal operation, the WILDCAT first wall design should achieve a 20-y lifetime regardless of the plate constraint. The primary limit on lifetime is the sputtering loss of the beryllium cladding. In the case of the plate which is allowed to expand but not bend, stresses are relatively low, and the lifetime could probably be substantially increased by increasing the beryllium thickness. Since the stresses are already high for the totally constrained plate, it is probably not advisable to increase the beryllium

thickness because of the additional thermal strains that would result. The greatest uncertainty in this analysis is the behavior of the bond between the beryllium and PCA. Experimental work is required to evaluate this behavior. Off-normal events such as disruptions or loss of coolant accidents could possibly lead to failure of radiation embrittled material. Additional work is also needed in this area.

REFERENCES FOR CHAPTER 4

1. R. F. Mattas, "Fusion Component Lifetime Analysis," ANL/FPP/TM-160, Argonne National Laboratory (1983).

2. C. C. Baker, et al., "STARFIRE - A Commercial Tokamak Fusion Power Plant Study," ANL/FPP-80-2, Argonne National Laboratory (1980).

3. D. L. Smith, "Physical Sputtering Model for Fusion Reactor First-Wall Materials," J. Nucl. Mater. 75, 20 (1978).

4. D. L. Smith, "Analytical Expressions: Physical Sputtering," Proc. Workshop on Sputtering Caused by Plasma Surface Interactions, Argonne National Laboratory, CONF-790775 (1979).

5. K. Evans, Jr., et al., "WILDCAT: A Catalyzed D-D Tokamak Reactor," ANL/FPP/TM-150 Argonne National Laboratory (1981).

Chapter 5

TRITIUM-RICH STARTUP EFFECTS

5. TRITIUM-RICH STARTUP EFFECTS

During startup of a D-D reactor it is convenient to add extra tritium to heat the plasma to ignition. This is done to heat the plasma via the D-T reaction and thereby to greatly reduce the rf heating requirements. As a result, however, there is a peak in the thermal power and wall loading during the plasma initiation as shown in Figs. 5-1 and 5-2 for the pulsed and steady-state versions, respectively, of WILDCAT. The peak level of ~4000 MW for pulsed use is 60% above the final operating power level, and there is some concern that this additional power could reduce the lifetime of the first wall and limiter if high stresses and strains are produced. The average wall loading during the power peak is 3.2 MW/m^2 compared with 1.5 MW/m^2 during the burn period.

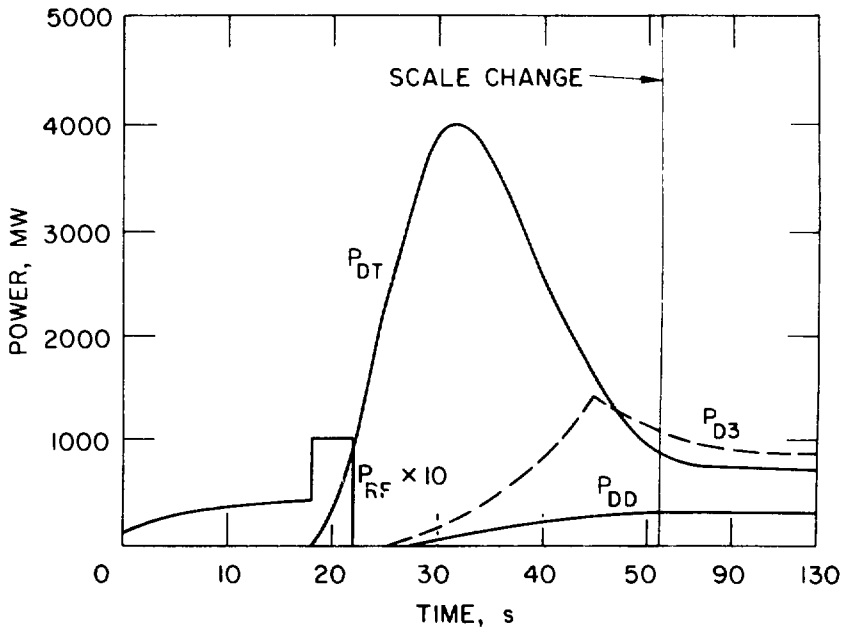

Fig. 5-1. Fusion powers and rf heating for the pulsed version of WILDCAT.

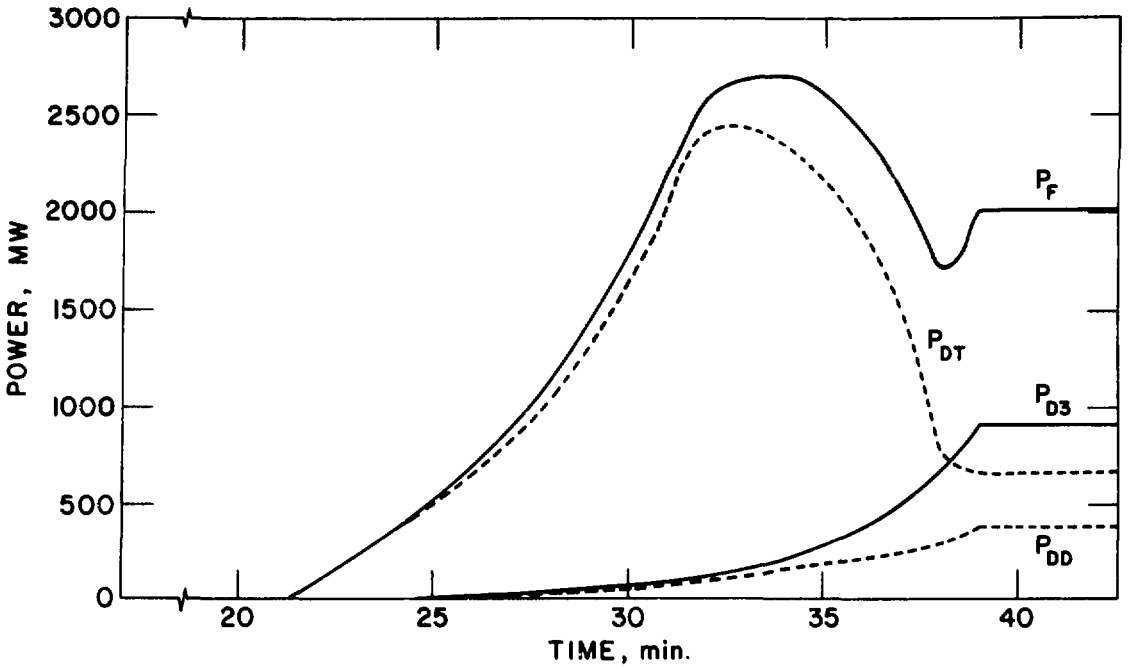

Fig. 5-2. D-T, D-D, D-^{3}He, and total fusion power during startup for the steady-state version.

The major concern for the first wall and limiter components, however, is the surface heat flux levels, since most of the heat deposited during normal operation is in the form of surface heating rather than bulk neutron heating. It is important to note, therefore, that the estimated surface heat flux during the power peak is only 0.6 MW/m^2 (~20% of the D-T wall loading) compared with 1.0 MW/m^2 during the burn cycle. The stresses and temperature produced in the first wall and limiter are in fact less during the power peak than during normal operation, and therefore, no additional problems are anticipated for the startup.

In the steady-state version, for which the startup is not so critical, the amount of tritium added was reduced, reducing the D-T power peak to ~2700 MWt with a wall loading of 2.2 MW/m^2 of which 0.4 MW/m^2 is heat load. Coupled with the greatly reduced frequency of starting up, these levels should be even less likely to be a problem.

Chapter 6

HIGH-FIELD MAGNET SUPPORT

6. HIGH-FIELD MAGNET SUPPORT

6.1 Support Against Out-of-Plane Forces

The support of a TF coil system against out-of-plane forces from the poloidal field coils is one of the most serious problems encountered in a tokamak reactor design. It has caused great problems in the INTOR and FED design studies, particularly because of fatigue problems in those two reactors, which are designed for a lifetime of order one million pulses. The out-of-plane forces and overturning moments, 1.5 GNm per TF coil, also presented major support problems in the STARFIRE design study,[1] although as a steady-state reactor, STARFIRE did not have the added problem of fatigue lifetime. These problems become even greater for WILDCAT with its larger overturning moment. The out-of-plane forces on the outer leg of a WILDCAT TF coil exert an overturning moment of 3.9 GNm. The out-of-plane forces on the curved portion of the inner leg are in the opposite direction and exert an overturning moment of -1.2 GNm. Thus, the net overturning moment on each coil is 2.7 GNm. In addition to reducing the overall moment, the opposing moments, however, act to twist the coil out of a plane shape.

Two basic approaches can be taken to the support of superconducting TF coils against out-of-plane forces. In the first, adopted in the FED and INTOR studies, neighboring TF coils are joined together by cold (liquid helium temperature) structural members. In the second, adopted in the STARFIRE study, neighboring coils are joined by warm (room temperature) structural members, and warm-to-cold support structure is required inside each TF coil dewar. Cold support requires a dewar system enclosing the coil-to-coil supports as well as the TF coils. Even at the scale of FED and INTOR, such a dewar presents problems of accessibility, fabricability, and excessive cool-down time and cost. All of these problems become worse, and possibly prohibitive, for WILDCAT.

Warm support presents two design problems: the choice of the coil-to-coil support and the choice of the cold-to-warm support within each coil dewar. The cold-to-warm support elements must have a large cross-sectional area to transmit the massive forces at acceptable stress levels. Even for materials such as epoxy-fiberglass, which combine high mechanical strength

with low thermal conductivity, these support elements introduce intolerable heat leaks into the magnet system unless the elements are long.

In STARFIRE these support elements were given a length roughly equal to the width of a TF coil by making the elements epoxy-fiberglass (G-10) tie bars connected to the vacuum tank at one side of the coil and to the helium vessel at the opposite side as shown in Fig. 6-1. Pivoting end-hooks eliminated bending moments in the tie bars from differential thermal contraction. In STARFIRE 17,000 of these tie rods were required. This same concept has been adopted for WILDCAT. It is the one which allows the greatest length to the support members without unduly adding to the overall size of the TF coil system or itself degrading accessibility between coils. However, the concept can be criticized because the tie bars support only in tension and provide no support in an off-normal situation in which the out-of-plane force changes direction.

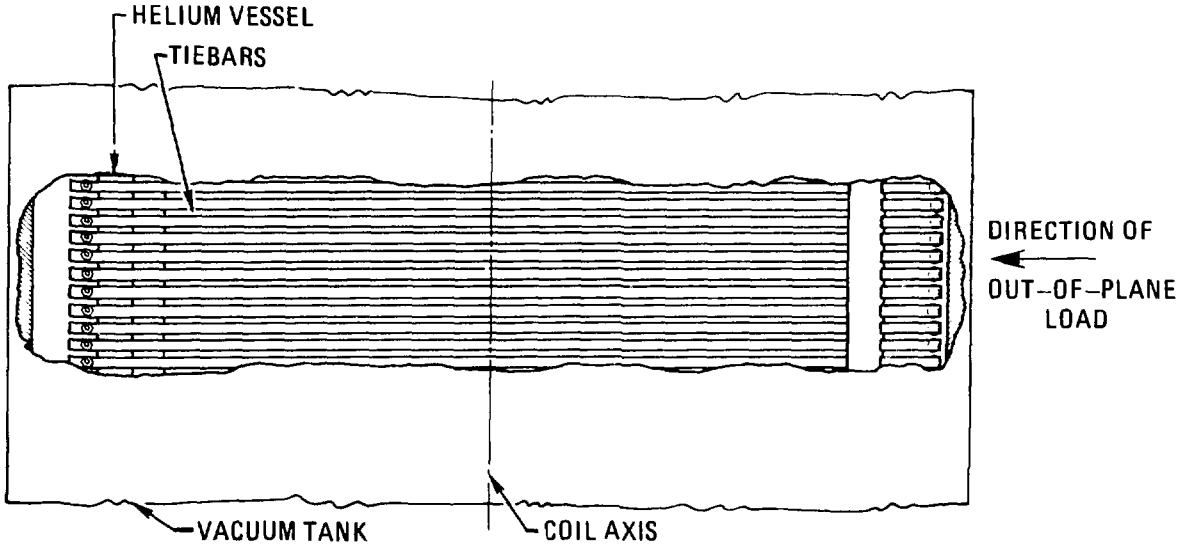

Fig. 6-1. Cutaway view of one coil showing support bars in high load region.

The coil-to-coil supports must also be addressed. In STARFIRE shear panels provided this support, but these did not appear scalable to the higher force levels of WILDCAT. For WILDCAT a support system has been adopted which essentially fills the space between TF coils with support material. Parts of the support system are removable with acceptable convenience to permit removal of a blanket sector.

Several possible materials for the support are compared in Table 6-1. The table gives material costs per sector, but fabrication costs are expected to be roughly proportional to the material costs. Reinforced concrete is seen

Table 6-1. Comparison of Candidate Materials for Coil-to-Coil Support

Material	Electromagnetic Considerations	Comparison for Similar Loading (tons/section)	Material Cost per Sector ($)	Shielding Quality
Concrete (reinforced)	Insulator	474	9,500	Good neutron
Aluminum	Requires insulation breaks	97.2	97,000	Fair gamma ray
Stainless steel, nonmagnetic	Requires insulation breaks	212	424,000	Good gamma ray
G-10 glass epoxy	Insulator	96.6	250,000	Fair neutron
1020 steel	Magnetic and requires insulation breaks	232	186,000	Good gamma ray

to be by far the least expensive, and also has desirable electromagnetic and fabrication properties. A concrete support may also serve as a biological shield against neutrons, but that effect has not been taken into account elsewhere in the shielding analysis of WILDCAT.

The reinforced concrete coil-to-coil support is shown in Figs. 6-2 and 6-3. Each sector consists of three blocks; only the central block needs to be removed to gain access to the blanket and shield region and only the plug needs to be removed to gain access to the limiter alone. Square keys 20 cm on a side and of full depth provide alignment and transfer the shear from the overturning moments. Because of concrete's weakness under shear, each block is entirely contained in a steel can with additional steel in regions of high shear stress such as around the shear keys.

Caveats which have been raised[2] recently about the difficulty of achieving adequate dimensional precision when using concrete in a fusion reactor should not apply to concrete entirely encased in a steel can.

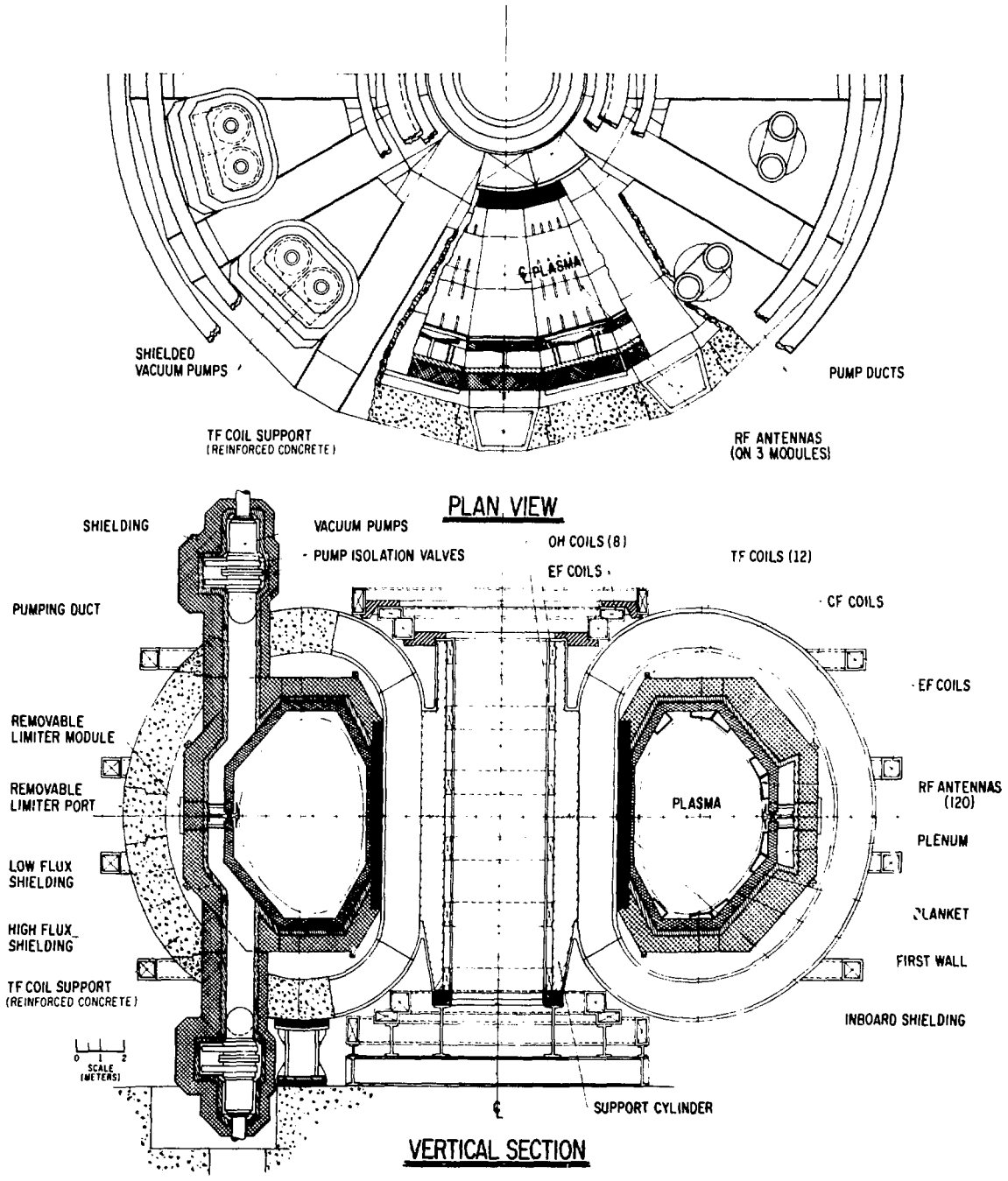

Fig. 6-2. WILDCAT

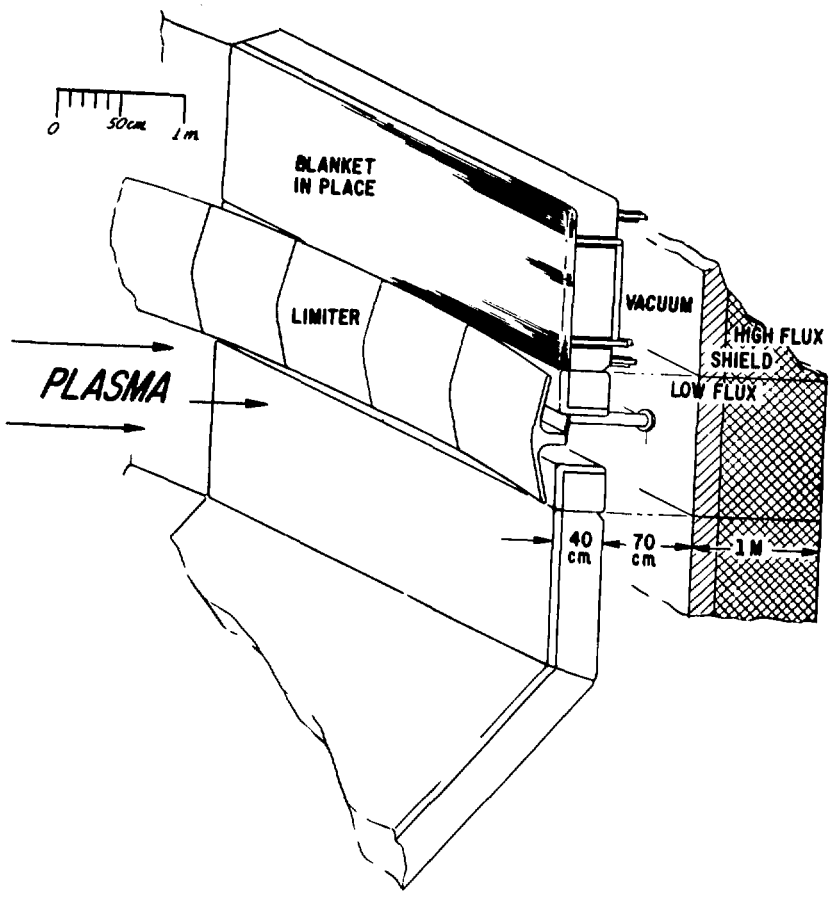

Fig. 6-3. Mechanical configuration of the limiter and the adjacent first wall, blanket, and shield.

REFERENCES FOR CHAPTER 6

1. C. C. Baker, et al., "STARFIRE - A Commercial Tokamak Fusion Power Plant Study," ANL/FPP-80-1, Argonne National Laboratory (1980).

2. E. Willough, "Interfacing Between Concrete and Steel Construction and Fusion Research Devices," Proc. 9th Symp. on Engineering Problems of Fusion Research, IEEE Pub. No. 81CH1715-2-NPS, Vol. I (1981), p. 37.

Chapter 7

REACTORS WITH LESS THAN FULL TRITIUM BREEDING

7. REACTORS WITH LESS THAN FULL TRITIUM BREEDING

7.1 Introduction

The two commercial, tokamak, reactor studies, STARFIRE[1] and WILDCAT,[2] represent the extremes of a continuum of possible reactor designs parameterized by the relative tritium content, $r_T = \bar{n}_D/\bar{n}_T$, of the plasma. STARFIRE has $r_T = 1.0$, the choice which optimizes the plasma performance given that sufficient tritium can be bred to maintain this value. WILDCAT has $r_T = 4.8 \times 10^{-3}$, the value that naturally occurs for a Cat-D device where no tritium is bred but all of the tritium produced by the reaction, D + D → p + T, is eventually burned in the plasma, either before it diffuses out or after it is reinjected. A summary of important parameters for STARFIRE and WILDCAT is shown in Table 7-1.

Table 7-1. Comparison of Steady-State D-T and Cat-D Reactor Designs

	STARFIRE	WILDCAT
Fuel cycle	D-T	Cat-D
$r_T = \bar{n}_T/\bar{n}_D$	1.0	4.8×10^{-3}
Major radius, m	7.0	8.58
Aspect ratio	3.6	3.25
Peak toroidal field, T	11.1	14.35
Plasma toroidal beta	0.067	0.11
Average electron temperature, keV	17.3	30.0
Plasma current, MA	10.1	29.9
Thermal power, GWt	4.0	2.9
Net electric power, MWe	1200	810
Tritium inventory, g	11,397	45
Normal tritium release, Ci/d	13	0.31
Cost of electricity, mills/kWh	35.1	62.8

STARFIRE and D-T reactors in general have the advantages of higher power density, lower $n\tau$ for ignition, and lower plasma temperatures, leading to more attractive performance and lower cost of electricity. WILDCAT and Cat-D reactors eliminate the problems associated with breeding tritium and have greatly reduced tritium inventories and tritium releases. In addition, the inboard

blanket/shield can be made thinner and significantly higher neutron energy multiplication can be obtained. It is interesting to look at reactors with intermediate values of r_T for several reasons: First, it may not be possible to breed sufficient tritium to maintain $r_T = 1$. Such tritium breeding, even though it is indicated in most D-T reactor designs, is a far from demonstrated fact. For example, liquid lithium blankets suffer from safety, corrosion, and pumping problems, and tritium extraction may be difficult for solid breeders. One, hence, may be forced to values of $r_T < 1$, especially in near-term designs. Second, it is possible that for some applications the best design might be an intermediate one, trading off the various advantages and disadvantages of the two extremes. Third, examination of the intermediate cases results in a better understanding of both the D-T and D-D cases and the factors which distinguish them.

The purpose of this study is to examine a number of intermediate cases between and including a D-T reactor as much as possible like STARFIRE and a Cat-D reactor as much as possible like WILDCAT. Relatively detailed designs will be developed so that reasonably accurate costs can be determined. The reactor subsystems will be modeled in such a way that their important parameters can be scaled to a large extent from STARFIRE and WILDCAT using a consistent set of design philosophies and assumptions.

Previous work has been done by Greenspan[3] on the concept of adding tritium to a Cat-D plasma (tritium-assisted operation) in order to reduce the ignition requirements and increase the fusion power density. However, the results were generic in nature and details of the full reactor designs were not undertaken. Conn[4] and Cohn[5] have also noted that there may be a continuum of reactors with $r_T < 1$ between D-T and Cat-D.

The work presented here is that done in the first part of this study. The calculation of specific reactor designs and their analysis is not covered, nor is the neutronic analysis. The complete work will be published in a later, separate report.

7.2 Reactor Design Criteria and Design Tradeoffs

The STARFIRE and WILDCAT tokamak reactor designs are used as the basis for our study. However, these two designs are not totally consistent with each other (with respect to choice of beta, choice of operating temperature, etc.,

see Table 7-1), and so some standardization has been made. Without standardization the effects of changes in r_T (or tritium breeding ratio) can be masked by inconsistent assumptions.

The first assumption that is made is to choose β_t = 10% for all the reactors including the D-T and Cat-D base design reactors. The reason for taking a consistent value for beta is that it is not felt that beta is a design choice. Any reactor would operate at the highest practical value of beta, which is not known at this time, and that value should be about the same for all reactors with similar cross sections and aspect ratios. For STARFIRE β_t was 6.7% and for WILDCAT it was 11%. Hence, the fusion power density of our D-T reactor is higher than that of STARFIRE, and that of the Cat-D reactor is somewhat lower than that of WILDCAT. Other MHD parameters, such as aspect ratio, safety factor, and D-shapedness, differ slightly between STARFIRE and WILDCAT. We have chosen a consistent set of MHD parameters for our study. These include aspect ratio, A = 3.25; elongation, κ = 1.6; D-shapedness, d = 0.2; safety factor, q(a) = 3.0 and q(0) = 1.0; and pressure profile exponent, α_p = 1.4.[6] These values are for the most part those of WILDCAT and are felt to be more general than those of STARFIRE, which were chosen to optimize the lower-hybrid current drive in that device. The less D-shaped plasma cross section makes the equilibrium field coil design easier, and probably does not detract greatly from the possibility of achieving a high beta.

The heat load on the first wall has been found to be a limiting design constraint for both STARFIRE and WILDCAT. Hence, we choose the same design criteria, that all radiation and changed particles emitted from the plasma not contribute more than 1 MW/m^2 to the first wall loading. As a consequence, the total first wall loadings (including neutrons) for our D-T and Cat-D designs are insignificantly different from those of STARFIRE and WILDCAT, respectively.

Total thermal power (plasma plus blanket) has been fixed at 4000 MWt for our designs. This is the same as for STARFIRE but greater than for WILDCAT (2915 MWt). This size plant was chosen for STARFIRE as being that typically desired by utility companies.[1] This assumption is desirable (though not essential) to facilitate comparison between designs. It has the effect of increasing the size of the Cat-D plant relative to WILDCAT.

Other general guidelines followed for STARFIRE and WILDCAT have also been observed here. These include fixing a maximum toroidal field strength of ~14.5 T and the assumption of steady-state operation.

The current drive method has been assumed to be relativistic electron beams (REB) as postulated for DEMO.[7] An REB system is predicted to be highly efficient and does not heat the plasma significantly in order to drive the current. There is some preliminary experimental evidence supporting REB current drive, but like all current drive schemes, it should be considered as speculative. STARFIRE used a lower-hybrid-wave, current drive, which is too inefficient for a D-D reactor, and WILDCAT used Alfven waves, which are somewhat more speculative, for current drive. The REB system, if it works, would be more attractive in both cases. The alternative to a steady-state, current drive, a pulsed, ohmically driven device, has many disadvantages, including significantly higher cost due to the large power supplies and required thermal storage as documented in the WILDCAT study.[2]

The impurity level of beryllium (from the pumped limiter) in the plasma has been set at 3% as was used in the previous designs. For the most part all other systems have been assumed to be similar to STARFIRE and WILDCAT, involving parameters intermediate to the two designs.

Shown in Table 7-2 is a listing of some of the major design tradeoffs one is expected to observe as r_T is decreased from unity (D-T reactor) toward a low value corresponding to operation in a Cat-D mode. These, in general, are the same design advantages and disadvantages observed for WILDCAT when compared to STARFIRE. One of the major contributions of this study is to determine quantitatively where the tradeoffs occur. One of the important positive effects of a reduced tritium concentration is the ability to have a less thick inner blanket/shield. This was shown to be very beneficial in the design of WILDCAT (a 1-cm decrease in thickness resulted in an increase of ~1% in thermal power). The reduction in neutron flux is the most significant factor in the blanket/shield size reduction. In addition, with a lower required tritium breeding ratio one can increase the neutron energy multiplication by using materials which enhance this property (e.g. steel) rather than breeding material. Thus while ~40% of the total fusion power from a Cat-D plasma is from neutrons, the blanket energy multiplication in WILDCAT led to a neutron contribution of ~52% to the thermal power. Perhaps the most important advantage of operating with a reduced tritium breeding ratio is the resulting reduced tritium inventory. However, even for a D-D reactor, the tritium permeates the reactor system and must be controlled. The level for which tritium becomes of

Table 7-2. Design Tradeoffs

Observed when $r_T = \bar{n}_T/\bar{n}_D$ is decreased from D-T toward Cat-D operation. Total thermal power, wall load, and β_t are fixed.

Positive Effects	Negative Effects
• Tritium breeding ratio (decreased)	• Fusion power density (decreased)
• Inner blanket and shield thickness (decreased)	• Toroidal magnetic field (increased)
• Neutron energy multiplication (increased)	• Plasma size (increased)
• Tritium inventory (decreased)	• Plasma operating temperature (increased)
• Tritium release (decreased)	• Ignition margin (decreased)
• Neutron fraction of total power (decreased)	• Required $n\tau$ (increased)

negligible concern is still a somewhat open question. In this report the tritium inventory is calculated as a function of r_T, and significantly low values are noted.

The negative effects of plasma operation with depleted tritium are also shown in Table 7-3. The most important of these is the reduction in fusion power density. The resulting power loss can be made up in essentially two main ways: (1) by increasing the toroidal field via stronger magnets or thinner inboard blanket/shield (the power is proportional to the fourth power of the field); and (2) by increasing the plasma size (the power is proportional to the plasma volume). The beneficial effects of a thinner blanket/shield and higher neutron energy multiplication, while helpful, do not significantly restore the lowered power density. The required increases in magnetic field and size, then, eventually lead to a higher cost of electricity.

7.3. Method of Analysis

The same general procedure used to design both STARFIRE and WILDCAT is followed here. A profile-averaged, steady-state, reactor analysis code,

Table 7-3. First-Wall/Blanket/Shield Model

Inside (10% of total volume):		
First wall	1 cm	65% PCA + 35% H_2O
Blanket	30 cm	90% PCA + 10% H_2O
Shield	x cm	15% Fe-1422 + 15% TiH_2 + 10% B_4C[a] + 55% W[a] + 5% H_2O
Outside (90% of total volume):		
First wall	1 cm	65% PCA + 35% H_2O
Blanket		
Li case	y cm	10% PCA + 90% Li[b]
	(70-y) cm	90% PCA + 10% H_2O
Li_2O case	y cm	10% PCA + 80% Li_2O[c] + 10% H_2O
	(70-y) cm	90% PCA + 10% H_2O
Shield	150 cm	60% Fe-1422 + 35% B_4C[a] + 5% H_2O

[a]95% theoretical density (T.D.).

[b]100% T.D., natural lithium.

[c]70% T.D., natural lithium.

TRAC-II, is used to determine the basic plasma parameters. Specified profiles are averaged over to obtain the global multispecies particle and energy balance equations solved by TRAC-II. The averaging is done over the actual flux surface of the MHD equilibrium, and the power and particle balance and the MHD equilibrium are handled consistently. A charged particle slowing-down model calculates energy deposited in thermal ions or electrons by superthermal fusion products. Superthermal fusions are also accounted for. A detailed toroidal field coil model is used to size the toroidal field superconducting magnets.[8] The TRAC-II code was also used for the STARFIRE and WILDCAT designs.

The neutronics analysis for calculation of the tritium breeding ratio and shielding requirements will employ the one-dimensional code ANISN[9] with the S_8P_3 approximation. The cross-section libraries for the particle transport[10] and the nuclear response function[11] used for the analysis will consist of 46 neutron groups and 21 gamma groups. The reactor activation analysis will be performed by RACC[12] based upon the Gear stiff matrix method.[13]

In addition, a detailed cost algorithm will be developed for this study. The costing will be done on the same basis and with the same assumptions as for STARFIRE and WILDCAT. The costs obtained should be directly comparable to those obtained for STARFIRE and WILDCAT.

7.4. Reactor Designs

We begin by first relating the plasma tritium concentration, $r_T = \bar{n}_T/\bar{n}_D$, to the tritium breeding ratio (TBR), which is defined as the net number of tritons burned in the plasma divided by the total number of neutrons (including both 14.06-MeV and 2.45-MeV neutrons) produced in the plasma. For a steady-state system in which all the tritium that diffuses out of the plasma is recycled or reinjected, an approximate expression for the TBR as a function of r_T and the ion temperature is

$$\text{TBR} \approx \frac{r_T\langle\sigma v\rangle_{DT} - (1/2)\langle\sigma v\rangle_{DD}^{T}}{r_T\langle\sigma v\rangle_{DT} + (1/2)\langle\sigma v\rangle_{DD}^{n}}, \qquad (7\text{-}1)$$

where $\langle\sigma v\rangle_{DT}$, $\langle\sigma v\rangle_{DD}^{T}$, and $\langle\sigma v\rangle_{DD}^{n}$ are the reactivities for the D-T, D-D (T branch) and D-D (n branch) fusion reactions, respectively. Equation (7-1) assumes a uniform plasma (i.e. ignores profile effects) and neglects superthermal fusions. Shown in Fig. 7-1 is a plot of this expression for the TBR versus r_T for various assumed ion temperatures. The TBR is fairly constant until r_T becomes less than ~ 0.05. The value of r_T must be less than 0.1 (for $T_i \lesssim 40$ keV) before the TBR is less than <0.9. Alternately, it could be stated that r_T is a very sensitive function of TBR for high-values of the TBR. Unfortunately, because of this behavior a relatively small decrease in TBR near TBR = 1.0 results in a severe decrease in D-T fusion power from the plasma.

Several other features of Fig. 7-1 should also be noted. For a 50-50 D-T plasma ($r_T = 1$), the value of the TBR can be seen from Eq. (1) to be slightly less than unity (TBR = 0.9944, at $T_i = 7$ keV). The reason is that a small number of tritons and a small number of neutrons are produced in the plasma from D-D reactions. If D-D reactions were ignored, the TBR would exactly be unity. For the case of Cat-D for which the TBR is zero, the value of r_T is seen to be a function of T_i. (For WILDCAT $r_T = 4.8 \times 10^{-3}$.) Actual values of

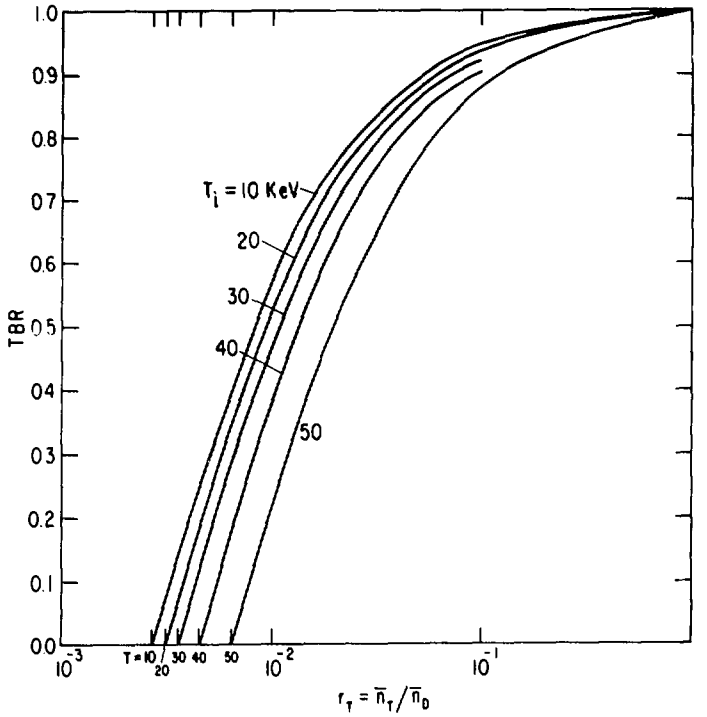

Fig. 7-1. Approximate expression for the tritium breeding ratio as a function of tritium concentration.

TBR versus r_T as used in the remainder of this paper also account for the temperature and density profile effects and superthermal fusions which are not included in Eq. (7-1). The criteria for determining an optimum plasma operating temperature as a function of r_T is discussed in the following paragraphs. The actual values of TBR versus r_T for the designs considered fall within the envelope of lines in Fig. 7-1 for 10 keV $\leq T_i \leq$ 50 keV.

The optimum temperature at which to operate a reactor is a somewhat sensitive and complicated function of r_T. A D-T reactor, for example, typically has a minimum ignition temperature near 4 keV, and the power density peaks near 7-8 keV. STARFIRE, on the other hand, was designed with an electron temperature of 17 keV. The reason was that at this temperature the lower-hybrid-wave, current drive is sufficiently more effective, modifying the desire to achieve maximum power density. For the more efficient current drive assumed in this work, however, it should not be necessary to choose a temperature much different from that for which the power density is a maximum. For WILDCAT, the temperature for which the power density peaks and the minimum temperature for ignition (~25 keV) are the same. (The power density peak, based on the maximum of the reaction rates, would occur at a lower temperature if ignition

could be achieved there.) Consequently, WILDCAT is operated at a temperature of 30 keV, a few degrees above the minimum to provide a safety margin for operation.

These average temperatures depend on the density and temperature profiles. The temperature profile exponent, α_T, has been taken to be 1.1 and the density profile exponent, α_n, has been taken to be 0.3. This corresponds to a sharp temperature profile and a broad density profile, and the two are consistent with the fairly broad pressure profile, which has been choosen to optimize the achievement of high beta. (These choices are in lieu of determining the profiles with a transport code, a procedure that cannot be performed accurately until the relevant transport coefficients are known.) Definitions and further discusson of the effect of different profiles are treated in Refs. 2 and 14. It should be noted that the above choice of profiles is different from those for both STARFIRE and WILDCAT but is thought to be the most realistic case.

The minimum temperature for ignition and the temperature for which the peak power density occurs have been determined as a function of r_T. Typically the minimum temperature increases as r_T decreases, and below some value of r_T, the maximum power density is coincident with the minimum temperature. If all of the ^3He that diffuses out is lost, then there is a minimum value of r_T below which ignition does not occur. If a reactor with a lower value of r_T is desired, some of the ^3He must be reinjected. WILDCAT falls in this category, and a discussion of the reinjection of ^3He is presented in Ref. 2.

The behaviors of the minimum electron temperature for ignition and the electron temperature for which the power density peaks are shown in Fig. 7-2. (The ion temperature is typically slightly higher than the electron temperature.) Two cases are considered, one in which no ^3He is reinjected but 75% of the diffusion flux is assumed to recycle naturally at the wall (see Ref. 2 for a discussion of the recycling/diffusion model) and another in which all the ^3He that diffuses out is reinjected. The first case corresponds to a net recycling coefficient, $R_3 = 0.75$, and the second, to $R_3 = 1.00$. Even though reinjecting the ^3He is beneficial at low values of r_T, it is deleterious for values of r_T close to unity. In the latter cases the power density is higher and the optimum temperature is lower for a given value of r_T than if the ^3He is removed. The problem of the ^3He as ash overrides its benefit as a fusion fuel.

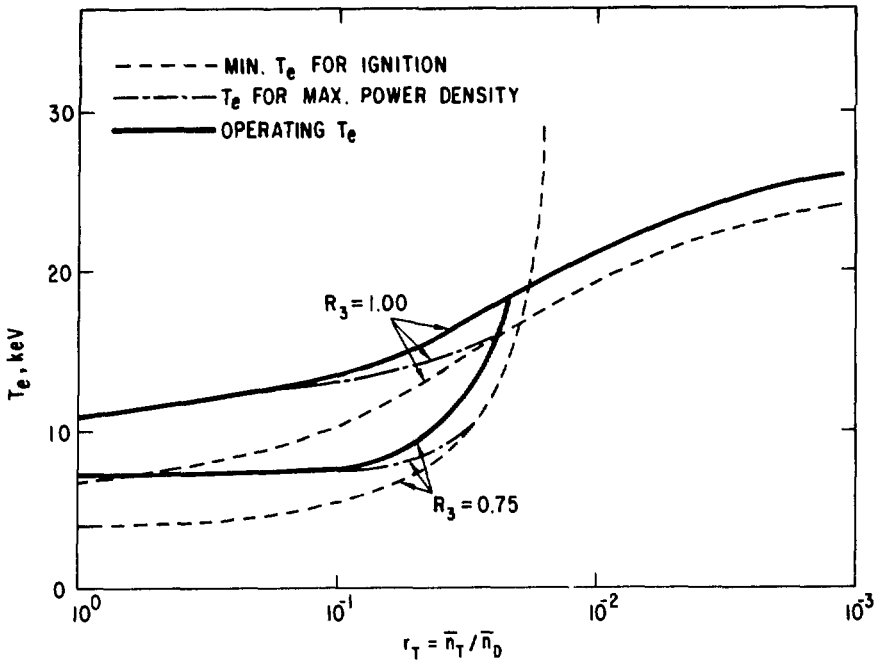

Fig. 7-2. Reactor temperatures as a function of r_T. The minimum temperature for ignition, the temperature for which the power density peaks, and the operating temperature for this study are shown. Catalyzation with respect to ^3He ($R_3 = 1$) is necessary for low values of r_T, but undesirable for values near unity. $R_3 = 0.75$ represents the wall recycling to be expected even if no ^3He is reinjected.

It is always advantageous to reinject any tritium that diffuses out, and the net tritium recycling coefficient, R_T, is always taken to be unity.

It can be seen from Fig. 7-2 that there are three regions to be considered in the r_T dependence of the temperature. In Region I with $1.0 \lesssim r_T \lesssim 0.1$ one would want to operate with ^3He removal at the temperature for which the power density peaks. This is typical of a D-T reactor. In Region III with $0.01 \lesssim r_T$ one would like to reinject all the ^3He and operate at a temperature as close as possible to the minimum temperature for ignition. This is typical of a Cat-D reactor. The intermediate Region II with $0.1 \lesssim r_T \lesssim 0.01$ is a transition region. The peak power density occurs near the minimum temperature for ignition and reinjection of the ^3He is becoming necessary. (It can be noted that if one wants to divert ^3He for "clean" D-^3He satellite reactors,[15] then r_T must be in Region I or II.

For the purposes of this study the operating temperature as a function of r_T has been taken to be the temperature for which the power density peaks or 2-3 keV above the minimum temperature for ignition, whichever is larger. The reactors are catalyzed in ^3He, that is R_3 is made unity, if necessary, but not otherwise, except that both catalyzed and uncatalyzed cases are investigated near the cross-over point, $r_T \simeq 0.03$. The chosen operating temperatures are shown in Fig. 7-3.

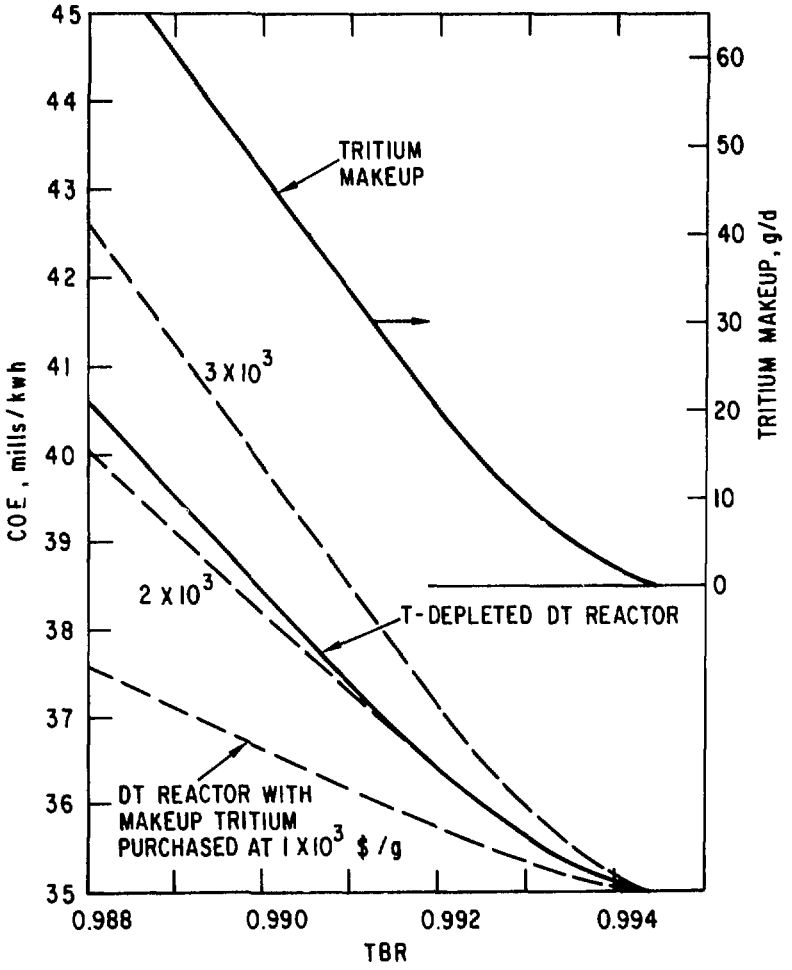

Fig.7-3. Comparison of the costs of energy for bred and purchased tritium.

7.5. Cost of Tritium

It is interesting to examine the cost penalty one pays in reactors with TBR $\lesssim$ 1, since uncertainties in many aspects of reactor design may force

operation in this regime. In Fig. 7-3, an approximate cost of energy (COE) is plotted as a function of TBR for 0.988 > TBR > 0.9944 or 1 > r_T > 0.1. The COE is approximated in a straightforward manner by assuming the STARFIRE COE (35 mills/kWh) at a TBR of 0.994 and adjusting the COE by the reduction in total reactor electric power as the TBR is decreased, keeping the size and magnetic field constant. Thus, the same capital equipment and operating costs are assumed, but only the generated electric power is decreased. This approximation should be valid in the regime close to STARFIRE. At a TBR of 0.988 the COE has risen to about 40.5 mills/kWh. Hence, a decrease in TBR of only 0.006 increased the COE by more than 5 mills/kWh (~15%). This is indeed a high price to pay for the slight inability to breed or recycle tritium.

Also plotted in Fig. 7-3 is the makeup tritium (in g/day) that is needed (in g/day) to operate at full 50-50 D-T (r_T = 1). If one were to purchase this tritium at 10^3, 2 × 10^3, or 3 × 10^3 \$/g (assuming availability from an outside vendor), then the COE would be as shown in Fig. 7-3 One might consider tritium-depleted operation if the cost of tritium is $\lesssim$2000 \$/g. Since the present (1982) cost of tritium is about 10^4 \$/g, it is unlikely that any tritium could be purchased at the needed low rates, so that the cost penalties of reduced TBR operation must be viewed as severe.

REFERENCES FOR CHAPTER 7

1. C. C. Baker, et al., "STARFIRE - A Commercial Tokamak Fusion Power Plant Study," ANL/FPP-80-1, Argonne National Laboratory (1980).

2. K. Evans, Jr., et al., WILDCAT: A Catalyzed D-D Tokamak Reactor, ANL/FPP/TM-150, Argonne National Laboratory (1981).

3. E. Greenspan and G. Miley, Nucl. Technol./Fusion 2, 590 (1982).

4. R. W. CONN, et al., "SATYR Studies of a D-D Fueled Axisymmetric Tandem Mirror Reactor," PPG-576, University California-Los Angeles (1981).

5. D. Cohn, Massachusetts Institute of Technology, personal communication (1982).

6. See Ref. 2 for the analytical form of the plasma boundary and exact definitions of the other MHD parameters.

7. C. C. Baker, et al., "A Demonstration Tokamak Power Plant Study (DEMO)," ANL/FPP-82-1, Argonne National Laboratory (1982).

8. L. A. Turner and M. A. Abdou, "Computational Model for Superconducting Toroidal Field Magnets for a Tokamak Reactor," ANL/FPP/TM-88, Argonne National Laboratory (1977).

9. "ANISN-ORNL: Multigroup One-Dimensional Discrete Ordinates Transport Code with Anisotropic Scattering," ORNL/RSIC-254, Oak Ridge National Laboratory (1973).

10. R. W. Rossin, et al., "VITAMIN-C: The CTR Processed Multigroup Cross Section Library fore Neutronics Studies," ORNL/RSIC-37 (ENDF-296), Oak Ridge National Laboratory (1980).

11. Y. Gohar and M. Abdou, "MACKLIB-IV: A Library of Nuclear Response Functions Generated with the MACK-IV Computer Program from ENDF/B-IV," ANL/FPP/TM-106, Argonne National Labortory (1978).

12. J. Jung, "Theory and Use of the Radioactivity Code RACC," ANL/FPP/TM-122, Argonne National Labortory (1979).

13. C. W. Gear, Numerical Initial Value Problems in Ordinary Differential Equations, Prentice-Hall, New Jersey (1971).

14. K. Evans, Jr., et al., "D-D Tokamak Reactor Studies," ANL/FPP/TM-138, Argonne National Laboratory (1980).

15. E. Greenspan and G. Miley, Nucl. Technol./Fusion 2, 43 (1982).

Distribution for ANL/FPP/TM-162

Internal:

M. Abdou
C. Baker
E. Beckjord
C. Boley
J. Brooks
F. Cafasso
Y. Cha
R. Clemmer
D. Ehst
K. Evans (5)
P. Finn
Y. Gohar
L. Greenwood
D. Gruen
A. Hassanein
C. Johnson
J. Jung
M. Kaminsky
S. Kim
Y-K. Kim
R. Kustom
R. Lari
L. LeSage
B. Loomis
S. Majumdar
V. Maroni
R. Mattas
B. Misra
R. Nygren
J. Roberts
D. Smith
H. Stevens
L. Turner
R. Wehrle
ANL Patent Dept.
FP Program (25)
ANL Contract File
ANL Libraries (2)
TIS Files (6)

External:

DOE-TIC, for distribution per UC-20, 20d (128)
Manager, Chicago Operations Office, DOE
Special Committee for the Fusion Program:
S. Baron, Burns & Roe, Inc., Oradell, NJ
H. K. Forsen, Exxon Nuclear Company, Inc., Bellevue, WA
M. J. Lubin, Standard Oil Company of Ohio, Warrensville Heights, OH
G. H. Miley, University of Illinois, Urbana
P. J. Reardon, Princeton University
D. Steiner, Rensselaer Polytechnic Institute
K. R. Symon, University of Wisconsin-Madison
K. Thomassen, Lawrence Livermore National Laboratory
Director, Science Applications, Inc.
R. Aamodt, Science Applications, Inc.
R. Alsmiller, Oak Ridge National Laboratory
D. Anthony, General Electric Company
R. Balzheizer, Electric Power Research Institute
D. Beard, DOE/Office of Fusion Energy
C. Blattner, McDonnell Douglas Astronautics Company
K. Blurton, Institute of Gas Technology
S. L. Bogart, Science Applications, Inc.
S. Buchsbaum, Bell Telephone Laboratories, Inc.
S. Burnett, GA Technologies
J. Butterworth, Culham Laboratory. UKAEA, England
G. Casini, Joint Research Centre, Ispra Establishment, Italy
R. Challender, UKAEA, Risley, England
C-H. Chen, Institute of Plasma Physics, People's Republic of China
F. Chen, University of California
R. Cherdak, Burns & Roe
S. Cohen, Princeton University
D. Cohn, Massachusetts Institute of Technology
R. Conn, University of California-Los Angeles
B. Coppi, Massachusetts Institute of Technology
R. Davidson, MIT Plasma Fusion Center

N. A. Davies, DOE/Office of Fusion Energy
J. Decker, DOE/Office of Fusion Energy
W. Dove, DOE/Office of Fusion Energy
H. Dreicer, Los Alamos National Laboratory
W. Drummon, University of Texas-Austin
D. Dobrott, Science Applications, Inc.
A. Dupas, Centre d'Etudes Nucleaires de Grenoble, France
W. Ellis, DOE/Office of Fusion Energy
R. Endicott, Public Service Electric and Gas Research Corporation
C. Finfgeld, DOE/Office of Fusion Energy
J. Foster, Jr., TRW, Inc.
T. Fowler, Lawrence Livermore National Laboratory
H. Furth, Princeton University
J. Gammel, St. Louis University
K. Gentle, University of Texas-Austin
J. Gilligan, University of Illinois (5)
J. Gordon, TRW, Inc.
S. Gralnick, Grumman Aerospace Corporation
D. Graumann, GA Technologies
E. Greenspan, NRCN, Israel
W. Grossman, New York University
B. Hall, Westinghouse R&D Center
W. Hagen, Science Applications, Inc.
R. Hagenson, Los Alamos National Laboratory
R. Hancox, Culham Laboratory, UKAEA, England
A. Haught, United Technologies Research Center
I. Hedrick, Grumman Aerospace
T. Hiraeoka, Japan Atomic Energy Research Institute, Japan
R. Hirsch, Exxon Research and Engineering Company
H. Horwitz, General Electric Company
R. Huse, Public Service Electric and Gas Company
A. Husseiny, Iowa State University
T. Jernigan, Oak Ridge National Laboratory
R. Johnson, General Dynamics - Convair
T. Kammash, University of Michigan
D. Klein, Westinghouse Electric Corporation
I. Knoblock, Max Planck Institute für Plasmaphysik, West Germany
J. Kokoszenski, Ralph M. Parsons Company
A. Kolb, Maxwell Laboratories
H. Kouts, Brookhaven National Laboratory
R. Krakowski, Los Alamos Scientific Laboratory
R. Langley, Sandia Laboratories
T. Latham, United Technologies Research Center
D. Leger, CEA-Saclay, Service DCAEA/SECF., France
R. Lengye, Max Plack Institute für Plasmaphysik, West Germany
H. Levin, GA Technologies
L. Lidsky, Massachusetts Institute of Technology
I. Maya, GA Technologies
J. McNally, Oak Ridge National Laboratory
R. Mills, Princeton University
O. Morgan, Oak Ridge National Laboratory
G. Moses, University of Wisconsin-Madison
L. Muhlestein, Hanford Engineering Development Laboratory

T. Nakakita, Toshiba Corporation, Japan
S. Naymark, Nuclear Services Corporation
D. Nelson, DOE/Office of Fusion Energy
T. Ohkawa, GA Technologies
E. Oktay, DOE/Office of Fusion Energy
D. Peterman, GA Technologies
R. Post, Lawrence Livermore National Laboratory
R. Pyle, University of California
M. Roberts, DOE/Office of Fusion Energy
A. Robson, Naval Research Laboratory
J. Rogers, Los Alamos National Laboratory
D. Rose, Massachusetts Institute of Technology
M. Rosenthal, Oak Ridge National Laboratory
R. Santoro, Oak Ridge National Laboratory
M. Sawan, University of Wisconsin
G. Sawyer, Los Alamos National Laboratory
P. Schmitter, Max Planck Institute fur Plasmaphysik, West Germany
K. Schultz, GA Technologies
R. Seale, University of Arizona
G. Shatalov, I. V. Kurchatov Institute of Atomic Energy, Moscow
W. M. Stacey, Jr., Georgia Institute of Technology
M. Stauber, Grumman Aerospace Corporation
L. Stewart, Princeton University
P. Stone, DOE/Office of Fusion Energy
S. Strausburg, GA Technologies
S. Tamor, Science Applications, Inc.
L. M. Waganer, McDonnell Douglas Astronautics Company, St. Louis, MO
R. Werner, Lawrence Livermore National Laboratory
L. Wittenberg, Monsanto Research Corporation
G. Woodruff, University of Washington
D. Young, Jr., University of Texas-Austin
M. Youssef, University of California-Los Angeles
Library, Centre de Etudes Nucleaires de Fontenay, France
Library, Centre de Etudes Nucleaires de Grenoble, France
Library, Centre de Etudes Nucleaires de Saclay, France
Library, Centre de Recherches en Physique des Plasma, Lausanne, Switzerland
Library, FOM-Institute voor Plasma-Fysika, Jutphass, Netherlands
Library, Comitato Nazionale per l'Energia Nucleare, Rome, Italy
Library, Joint Research Centre, Ispra, Italy
Library, Japan Atomic Energy Research Institute, Ibaraki, Japan
Library, Max Planck Institute fur Plasmaphytsik, Garching, Germany
Library, Culham Laboratory, UKAEA, Abingdon, England
Library, Laboratorio Gas Ionizati, Frascatti, Italy